

Study on the Biological Communities and Bioweathering of Marble Surfaces at the Altar of Prayer for Good Harvest in the Temple of Heaven (Beijing, China)

Youping Tian *

School of Earth Sciences and Resources, China University of Geosciences (Beijing), Beijing, China

Abstract: This study investigates the biological communities on the marble surfaces of the Altar of Prayer for Good Harvest in the Temple of Heaven, Beijing. The predominant populations are aerial cyanobacteria that thrive in calcareous environments, are drought-resistant, grow slowly, and have strong vitality. These aerial cyanobacteria exhibit different populations compositions depending on the orientation of the marble surfaces. On the east-facing, warm and humid surfaces, the biological communities are mainly composed of small filamentous cyanobacteria such as *Scytonema* sp.2 and coccoid cyanobacteria like *Gomphosphaeria* sp. On the west-facing, hot and humid surfaces, the biological communities are dominated by *Scytonema* sp.1, a small filamentous cyanobacterium, and mosses. On the north-facing, cold and humid surfaces, the biological communities primarily consist of coccoid cyanobacteria such as *Myxosarcina* sp. and *Gomphosphaeria* sp. On the south-facing, hot and dry surfaces, the biological communities are mainly composed of small or large filamentous cyanobacteria like *Scytonema* sp.1 and *Nostoc* sp.. The observed intensity of weathering varies with orientation: south > west > east > north, which is consistent with the weathering patterns observed on the cloud dragon heads in different orientations. The biological communities on the marble surfaces exhibits various colors, with gray-black being the most common, followed by gray-white, black, brown, and dark brown. The gray-black communities are primarily composed of *Myxosarcina* sp. and *Gomphosphaeria* sp.. The biological communities also display different morphologies,

* Corresponding author at: School of Earth Sciences and Resources, China University of Geosciences (Beijing), Beijing, China
E-mail address: typ@cugb.edu.cn (Y. Tian)

27 including membranous, hairy, carpet-like, leathery, shell-like, and powdery layers. The population
28 composition of these different morphological communities varies. The growth of aerial organisms
29 on the rock surfaces is controlled by both macro-hydrological dynamics and micro-surface
30 topography. On a macro scale, in areas with low rainfall intensity, the biofilm is sparse, and
31 bioweathering is weak. In areas with high rainfall intensity, "ink bands" rich in cyanobacteria form,
32 leading to strong bioweathering. On a micro scale, the micro-topographic features of the rock
33 regulate local hydrological conditions, determining the colonization patterns: rough, uneven
34 surfaces with discrete water films promote point-like biological aggregation, leading to the
35 development of solution pits; linear decorations or joint surfaces with directional water storage drive
36 linear biological expansion, forming solution traces and grooves; smooth, dense surfaces with
37 uniform water film coverage support planar biological growth, ultimately leading to the overall
38 detachment of the weathering layer. The mechanism of bioweathering involves aerial organisms
39 secreting organic acids, which dissolve inorganic salts in the rock, providing nutrients and gradually
40 "eating away" at the rock, destroying its surface structure, and causing progressive weathering.
41 Preventing or reducing the growth of aerial organisms is key to slowing down the bioweathering
42 process of the stone relics at the Altar of Prayer for Good Harvest.

43
44 Keywords : Altar of Prayer for Good Harvest, marble, aerial organisms, cyanobacteria,
45 bioweathering

46
47 **1. introduction**

48
49 The Hall of Prayer for Good Harvest, located in the Temple of Heaven in Beijing, China,
50 was completed in 1420. It served as the site for the emperors of the Ming and Qing dynasties to
51 perform the "Heaven Worship" and "Prayer for Good Harvest" rituals. It is also the largest
52 existing ancient architectural complex for heaven worship in the world. In 1961, the State
53 Council of China designated the Temple of Heaven as a "National Key Cultural Relic Protection
54 Unit." In 1998, it was recognized by UNESCO as a "World Cultural Heritage Site." The hall
55 covers an area of 460 square meters and is built on a three-tiered circular marble platform,
56 which is 6 meters high and surrounded by white stone balustrades. This platform is known as

57 the Altar of Prayer for Good Harvest (Fig. 1-a). The marble used in the construction is divided
58 into two types: White marble and Bluish-white marble. White marble, due to its fine texture and
59 ease of detailed carving, is often used in decorative parts such as balustrades and carvings.
60 Bluish-white marble, with its higher compressive strength (Ye and Zhang, 2019) and better
61 corrosion resistance compared to White marble (Qu, 2018), is typically used in load-bearing
62 and wear-resistant areas such as the base and paving. Most of the White marble and Bluish-
63 white marble used in the construction come from the marble quarries in Dashiwo Town,
64 Fangshan District, Beijing. (Wu and Liu, 1996; Lü and Wei, 2020). Compared to other types of
65 rock used in the Temple of Heaven complex (such as limestone, granite, and sandstone), the
66 marble used in the Altar of Prayer for Good Harvest is the most susceptible to weathering due
67 to its lower hardness. White marble, a special variety of marble, is particularly sensitive to
68 weathering (Ye and Zhang, 2019). Additionally, because marble is rich in calcium, it serves as
69 a preferred substrate for biological growth (Miller, et al., 2006). However, the organisms are
70 not uniformly distributed across the entire marble surface; their distribution is selective. In
71 addition to requiring a calcium-rich substrate, they also need water. In areas with low rainfall
72 intensity (such as high and protruding locations on the marble surface), where water is scarce,
73 there is little to no biological growth, and the surface appears white or yellowish-white with
74 minimal biofilm and weak bioweathering. In contrast, in areas with high rainfall intensity (such
75 as water convergence points, channels, and Chi Heads), where water is abundant, there is
76 extensive biological growth, and the surface appears black (with patches of brown and gray-
77 black) with a prominent biofilm and strong bioweathering. (Fig.1-b). The gradient distribution
78 of the biofilm on the rock surface is significantly spatially coupled with the variations in
79 instantaneous runoff, reflecting an optimal water allocation mechanism in arid environments
80 (Tian, 2004; Macedo, et al., 2009). In addition to the rock substrate and precipitation,
81 environmental factors such as wind and air pollution also influence microbial colonization, a
82 phenomenon known as "bioreceptivity" of vulnerable structural materials (Guillitte and
83 Dreesen, 1995; Miller, et al., 2012). Among these organisms, cyanobacteria are particularly
84 significant because they can grow with just light and water, and they can survive within the
85 rock, playing a crucial role in the degradation of stone cultural relics (C., Gaylarde, 2020).



a

b

87 **Fig. 1.** The Altar of Prayer for Good Harvest in the Temple of Heaven, Beijing, China, and
 88 the distribution of black biofilm on its marble surface.

89 a. The three-tiered circular marble platform surrounded by white stone balustrades below the Hall of Prayer for Good Harvest is known as
 90 the Altar of Prayer for Good Harvest; b The surface of the Altar of Prayer for Good Harvest marble is covered with black biofilm, which is
 91 distributed according to the intensity of rainfall. In areas with low rainfall intensity, the biofilm is not noticeable. In areas with high rainfall
 92 intensity (such as channels, water convergence points, and dragon heads), there is a significant distribution of black biofilm.

93

94 Black microbial distributions, forming black crusts, have been observed on marble surfaces in
 95 many regions (Checcucci, et al., 2022; Monte and Sabbioni, 1986; Praderio, et al., 1993; Gorbushina,
 96 et al., 2002). This phenomenon is also referred to as marble blackening (Moropoulou, et al., 1998),
 97 bioweathering, or biodeterioration. The microbial communities on marble surfaces exhibit high
 98 diversity (Timoncini et al., 2022). The black crust microbial communities are primarily composed
 99 of coccoid and filamentous cyanobacteria from the genera *Chroococcus*, *Gloeocapsa*, and
 100 *Tolypothrix* (Lombardozzi, et al., 2012), as well as green algae, fungi (Isola, et al., 2016; Leo, et al.,
 101 2019; Marvasti, et al., 2012), and lichens (Pinna, et al., 2018). *Chroococcus* can bore into the marble
 102 surface, demonstrating remarkable environmental adaptability: not only do they form blue-green
 103 biofilms on the rock surface (epilithic growth), but they also penetrate through cracks
 104 (chamomelitic growth), colonize mineral interstices (cryptoendolithic growth), and even
 105 actively excavate (euendolithic growth) deeper into the marble. The tubular tunnels drilled by
 106 *Chroococcus* in calcite crystals involve both chemical dissolution and mechanical erosion, making
 107 them a dominant species in the community (Golubić, et al., 2015; Scheerer, et al., 2009). Biofilms

108 alter the thermal and moisture properties of the material, exert colloidal mechanical stress, and
109 secrete acidic and redox metabolites, which intensify mineral lattice destruction and promote the
110 formation of harmful crusts (Guiamet, et al., 2013; Warscheid and Braams, 2000). They can also
111 accelerate rock weathering, leading to the formation of pits (Danin and Caneva, 1990) and control
112 the micro- and macro-morphology of the rock surface (Tian, 2004). Black biofilms on marble
113 surfaces show differential erosion based on orientation, such as differences between windward and
114 leeward faces (Danin and Caneva, 1990). Height differences also play a role, with height having a
115 greater impact on microbial weathering than orientation. The microenvironmental gradients on the
116 rock surface are the core driving factors for the biological erosion of stone cultural heritage (Trovão
117 and Portugal, 2024). In extremely arid environments, "gravel shell" microbial communities
118 composed of lichens, cyanobacteria, and fungi drive the decomposition of rock particles and the
119 formation of primitive soil (terrestrial protopedon) through bioweathering mechanisms such as pH
120 changes, swelling and shrinking, enzymatic activity, and mineral migration (Jung, et al., 2020). Even
121 in areas with fewer black biofilms, the frequency of microbial presence increases as the physical
122 and chemical acid erosion of marble forms a powdery layer, accelerating the transformation of
123 marble into soil and posing a serious threat to marble cultural heritage. Understanding the
124 bioweathering patterns on marble surfaces is crucial for the conservation of marble cultural heritage.
125 For example, targeted use of microbial methods to remove black crusts can be more effective than
126 purely chemical or laser methods (Gioventù, et al., 2011).

127 Current research on the weathering of marble cultural heritage in Beijing has primarily focused
128 on the roles of physical and inorganic chemical processes, such as acid erosion. Studies have found
129 that the surface peeling and pollution of the marble steles at the Confucian Temple in Beijing are
130 caused by acid rain erosion (He, 2021). Freeze-thaw cycles can lead to internal structural damage
131 in rocks, while salt fog crystallization causes pore expansion and degradation (Li, 2023).
132 Temperature changes affect the physical and mechanical properties of dolomitic marble in Beijing,
133 leading to surface peeling, dissolution of dolomite crystals, and the formation of crusts due to SO₂
134 and dust pollution (Liu, 2020; Zhang, et al., 2016; Wang, et al., 2022). The mechanism of granular
135 peeling on marble surfaces is attributed to the low amount of cementing material between particles,
136 resulting in weak cementation. Surface particles are disrupted by mining unloading, processing
137 damage, stress concentration, and temperature variations, leading to peeling (Wang, 2010).

138 Temperature fluctuations, acid rain dissolution, water erosion, and salt micro-crack filling are the
139 main causes of weathering in Fangshan marble in Beijing (Zhang, et al., 2015). Research on the
140 weathering of white marble components in the Hall of Supreme Harmony in the Forbidden City
141 indicates that thermal stress from solar radiation and rain erosion are the primary factors (Wu, et al.,
142 2023). It has been found that under the combined action of acid and salt, dolomite crystals degrade
143 through dissolution, interstitial erosion, and spalling. Salt crystallization accelerates the latter two
144 types of damage, while acid erosion promotes salt penetration, significantly increasing the rate of
145 degradation (Zheng, et al., 2025). Regarding bioweathering of marble in Beijing, only a few studies
146 have mentioned it (Beijing Institute of Ancient Architecture, 2018). The main types of damage to
147 marble in Beijing include fissures, peeling, disintegration, crust formation, solution pits, erosion,
148 component loss, discoloration, biological parasitism, and improper human restoration (Yang, 2016).
149 Two types of peeling in white marble in the Beijing area have been identified: one driven by the
150 synergistic effects of thermal weathering, lichen, and rainfall, and the other by acid rain and capillary
151 water absorption (Zhang, 2022). To understand the patterns of bioweathering in marble, it is
152 essential to know the composition, structure, and metabolic potential of the resident microbial
153 communities and their interactions with the stone (Pinna, 2017; Marvasti, et al., 2019). This study
154 focuses on analyzing the community composition, structure, and relative biomass of biofilms on the
155 marble surface of the Altar of Prayer for Good Harvest in Beijing. By identifying the development
156 process and patterns of the biofilm communities, we aim to reveal the mechanisms of biocorrosion
157 and provide a scientific basis for developing more targeted conservation strategies for marble
158 cultural heritage.

159

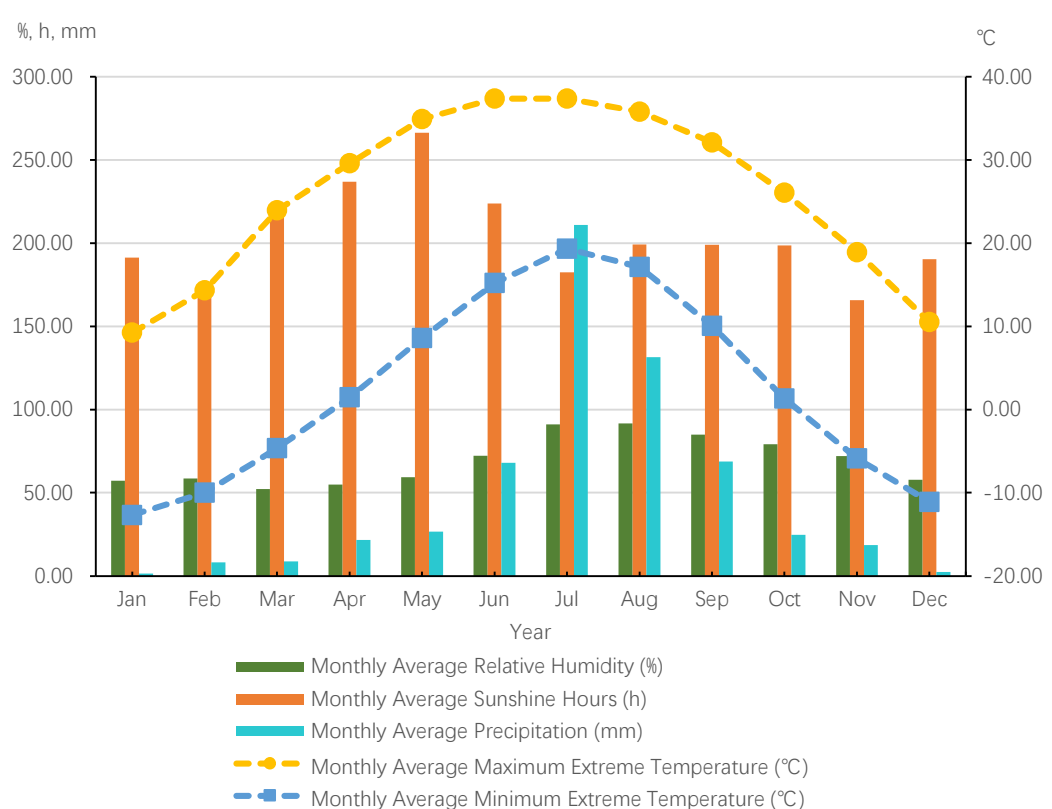
160 1. Overview of the Study Area

161

162 Beijing is located in a warm temperate monsoon semi-humid climate zone, characterized by a
163 cool mountain climate. The region has an average annual temperature of 10.8°C, with a frost-free
164 period of approximately 150 days. In winter, Beijing is influenced by cold air masses from the
165 northwest, resulting in a cold and dry climate. The prevailing wind direction during this season is
166 from the northwest, with an average annual wind speed of 1.9 meters per second. In summer, the
167 influence of the subtropical high-pressure system makes the climate hot, and rainfall is relatively

168 concentrated, especially from July to September, when about 85% of the annual precipitation occurs,
169 often in the form of heavy rain. Autumn in Beijing is generally pleasant, while spring is relatively
170 short. The frost-free period ranges from 190 to 200 days. Under extreme weather conditions, the
171 maximum summer temperature can reach 42°C, and the minimum winter temperature can drop to -
172 25°C. According to data from the National Meteorological Information Center of Beijing from 2009
173 to 2024, the annual precipitation in Beijing shows significant fluctuations (Fig. 2). There is no clear
174 trend in the annual average relative humidity and annual average precipitation, but there is an
175 increasing trend in the annual average sunshine hours and annual average extreme maximum
176 temperature, and a decreasing trend in the annual average extreme minimum temperature (Fig. 3).
177 During the period from 2009 to 2024, the multi-year average annual total rainfall was 610 mm.

178



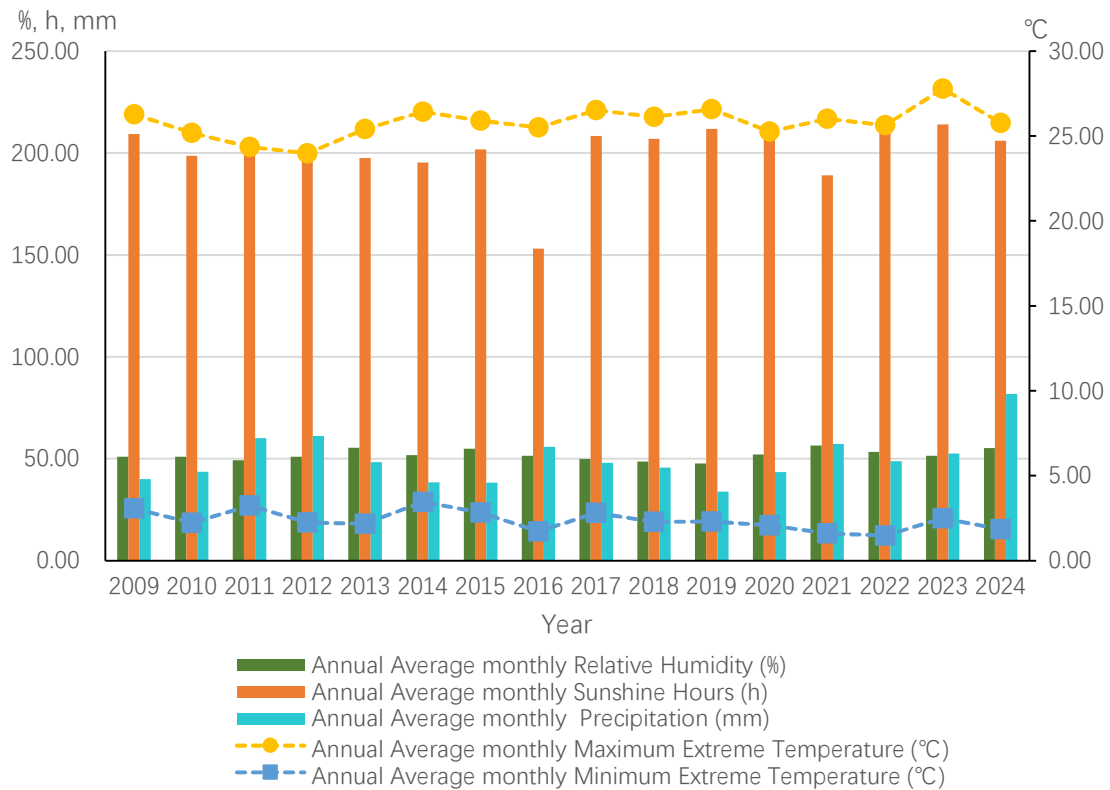
179

180

181 Fig. 2 Monthly average relative humidity, monthly average sunshine hours, monthly average precipitation,
182 monthly average extreme maximum temperature, and monthly average extreme minimum temperature
183 in the Beijing region from 2009 to 2024

184

(based on data from the National Meteorological Science Data Center Website).



187 Fig. 3 Annual average relative humidity, annual average sunshine hours, annual average precipitation, annual average extreme maximum temperature, and annual average extreme minimum temperature in the Beijing region from 2009 to 2024

188
189 (based on data from the National Meteorological Science Data Center Website).

193 The Altar of Prayer for Good Harvests at the Temple of Heaven is a triple-tiered circular altar
194 (Fig. 1-a). Each tier of its white marble base is adorned with 100 intricately carved Chi Heads (Fig.
195 1-b, Fig. 16). The Chi Head (Chi Shou) is a unique functional and decorative architectural element
196 in traditional Chinese architecture, inspired by the mythical hornless dragon-like creature "chi."
197 Resembling a dragon's head without horns, it is commonly found on the roofs, beams, columns, and
198 stone railings of palaces and temples. Its design integrates both aesthetics and practicality: rainwater
199 is channeled through hidden drainage holes in the Chi Heads, preventing water erosion of the base
200 while creating a distinctive visual effect. The three tiers of the altar collectively have a total of 300
201 Chi Heads, with the decorative themes progressively layered—dragon heads (dragon Chi Heads) on

202 the upper tier symbolize imperial authority, phoenix heads (phoenix Chi Heads) on the middle tier
203 represent auspicious harmony, and cloud patterns (cloud Chi Heads) on the lower tier reflect the
204 connection between heaven and earth. During the rainy season, water cascades from the mouths of
205 the Chi Heads on all three tiers, creating a spectacular sight of "dragons spouting torrents, phoenixes
206 holding pearls, and clouds rolling like waves." Over time, the weathering of the Chi Heads has
207 varied significantly depending on their orientation (Fig. 16), vividly illustrating the dynamic
208 interaction between ancient architectural elements and the natural environment.

209 The main production area for Beijing marble is Dashiwo Town, located in the southwestern
210 part of Fangshan District, Beijing. In the distribution of marble layers in Fangshan, Bluish-white
211 marble is the first to be quarried due to its shallow burial depth. On the other hand, White marble is
212 found in the deepest layer, with a burial depth that is usually the deepest among the stone layers,
213 ranging from 90 cm to 150 cm in thickness. In the construction industry, both White marble and
214 Bluish-white marble are widely used as marble materials.

215

216 2 Research Methods

217 2.1 Field Work

218 Different forms of biofilm communities on the marble surface were collected (biofilms are
219 loose and easily detachable, so a small amount was gently picked by hand without damaging the
220 cultural relics), placed in specimen boxes, numbered, and photographed. The appearance, color, and
221 morphology of the biofilms were described, and the date and location were recorded. The micro-
222 morphologies formed by the dissolution of the biofilm communities were observed and
223 photographed. A total of 40 biofilm community specimens were collected, and 22 photographs of
224 the field biofilm communities were taken. On clear, sunny days, the surface temperature of the rock
225 in the sampling area was measured using an infrared thermometer (DL333380, Deli, China). At the
226 same time, the degree of weathering of the Chi Heads was marked on the overhead view of the Altar
227 of Prayer for Good Harvests. Chi Heads with complete surface ornamentation were marked in green,
228 those with incomplete ornamentation were marked in yellow, and those with completely weathered
229 and disappeared ornamentation were marked in red. Environmental humidity in different directions
230 was measured using a hygrometer (THM-H1, Delixi, China).

231

232 2.2 Laboratory Work

233 2.2.1 Microscopic Observation

234 The size, morphology, and color of the biofilm communities were observed using a
235 stereomicroscope (Szx7, Olympus, Japan). Then, temporary slides were prepared from different
236 colored biofilm communities and observed under a biological microscope (Bx51, Olympus, Japan).
237 The species of the biofilm communities were identified (Desikachary, 1959; Geitler, 1932; Komarek,
238 1998, 2005, 2013; Zhu, 1991; Fott, 1980; Hu and Wei, 2006), and photographs were taken. For each
239 biofilm community ecological specimen, a microslide was prepared, resulting in a total of 40
240 microslides, and 142 microscopic photographs were taken.

241 2.2.2 Biomass Statistics

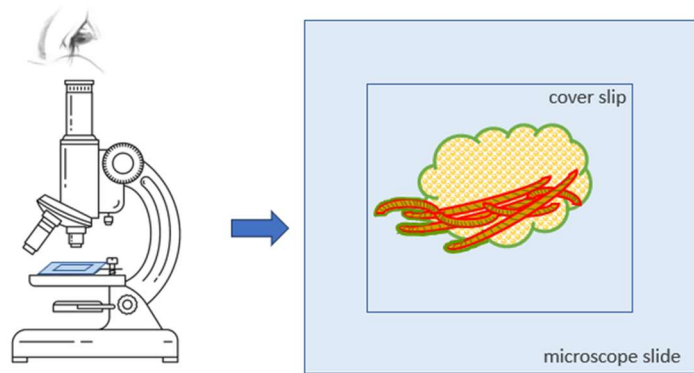
242 The volume percentage of the species in the biofilm communities was recorded. The volume
243 percentages of the species were statistically analyzed to calculate the relative volume (Vx, relative
244 biomass) and the relative volume percentage (Yx, relative biomass percentage). The statistical and
245 calculation methods are as follows:

246 (1) Relative Volume (Vx, Relative Biomass)

247 To obtain the relative volume, the following steps need to be taken:

248 1) Determine the volume percentage (v(x)%)

249 By estimating the percentage of the volume that each species occupies relative to the total
250 volume of all species in each microslide, the volume percentage (v(x)%) of that species in the
251 microslide is obtained. The estimation can be based on the area occupied by each species in the
252 microslide, as within the same microslide, the thickness between the cover slip and the slide is nearly
253 uniform across different areas. Therefore, under the same thickness, the larger the area occupied by
254 a species, the greater its volume (Fig. 4).

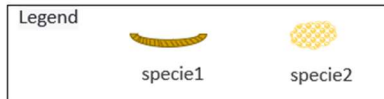


$$V(\text{Specie1})\% = \frac{\text{specie1 area} \times \text{high}}{(\text{specie1 area} + \text{specie2 area}) \times \text{high}} \times 100 \%$$

$V(\text{Specie1})\%$: volume percentage of specie1

area within the red line: specie1 area

area within the green line: specie1 area + specie2 area



255

256 Fig. 4 Visual Method for the volume percentage ($v(x)\%$) of a Specie
257 in a Biofilm Community Microslide

258 If there are two species in the microslide: Species 1 and Species 2, the volume percentage of Species 1 can be estimated by dividing the
259 area occupied by Species 1 by the total area occupied by both Species 1 and Species 2, and then multiplying by 100. This gives the volume
260 percentage ($v(x)\%$) of Species 1 in the microslide.

261

262 2) Sum the Volume Percentages

263 Add up the volume percentages of the same species across all microslides in the study area to
264 obtain the relative volume (Vx) of a species in the study area. The relative volume of a species
265 roughly reflects its relative biomass in the biofilm community of the study area. It does not represent
266 the actual volume but is an estimated relative value that is meaningful for comparison.

267

$$268 Vx = v(x)_{i_1} + v(x)_{i_2} + \dots + v(x)_{i_x}$$

269 i_x is the microslide number; x is a specific species ($x=a, b, c, \dots$); $v(x)_{i_x}\%$ is the volume percentage of
270 species x .

271 (2) Relative Volume Percentage (Yx , Relative Biomass Percentage)

272 This is the percentage of the relative volume (Vx) of a species in the biofilm community of the

273 study area relative to the sum of the relative volumes of all species in the biofilm community. It is
274 also referred to as the relative biomass percentage.

275

276
$$Y_x = \frac{V_x}{n \times 100} \times 100\%$$

277 n is the total number of microslides.

278

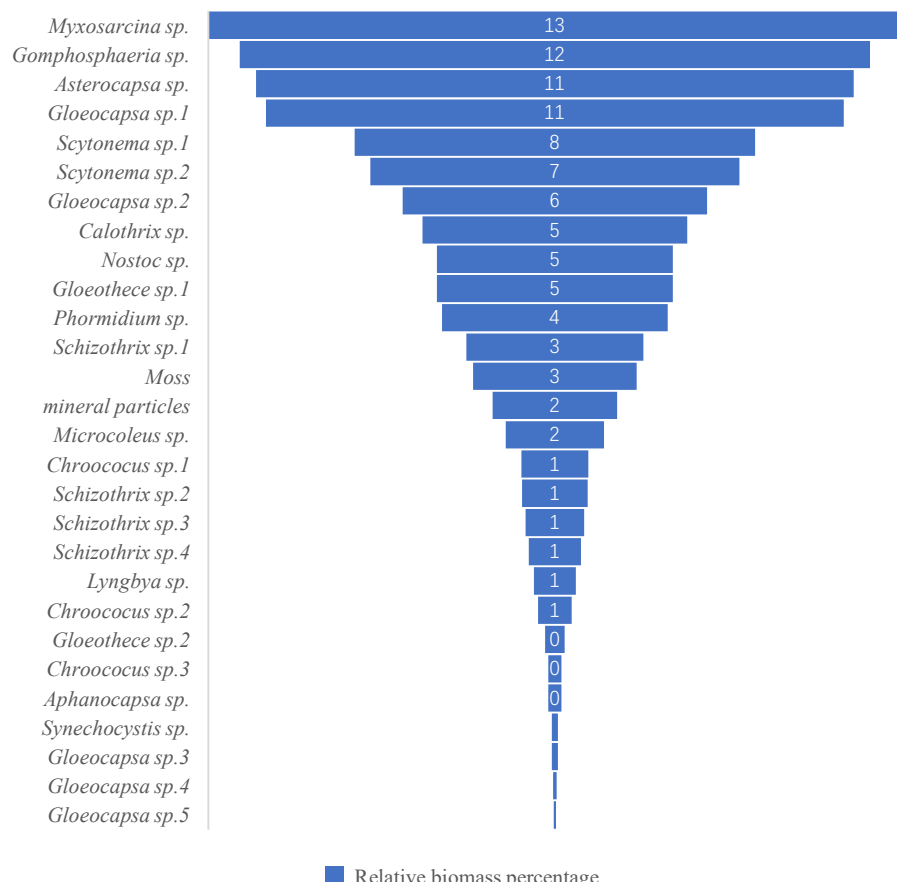
279 The relative volume percentage, also known as the relative biomass percentage, does not
280 represent the actual biomass. This is because it is currently very difficult to accurately measure the
281 biomass of biofilm communities on marble rock surfaces. By estimating through microscopic
282 observation, one can get a rough understanding of the growth status of the biofilm community. It is
283 a relative value and is meaningful only for comparative purposes.

284

285 3 Results

286 3.1 Distribution of communities in the Study Area

287 The composition of the biofilm communities on the marble surface in the study area includes
288 a total of 30 genera and species (Fig. 5). The most abundant species is *Myxosarcina* sp., followed
289 by *Gomphosphaeria* sp., *Asterocapsa* sp., *Gloeocapsa* sp.1 (Fig. 6), and *Scytonema* sp.1, among
290 others.



■ Relative biomass percentage

291

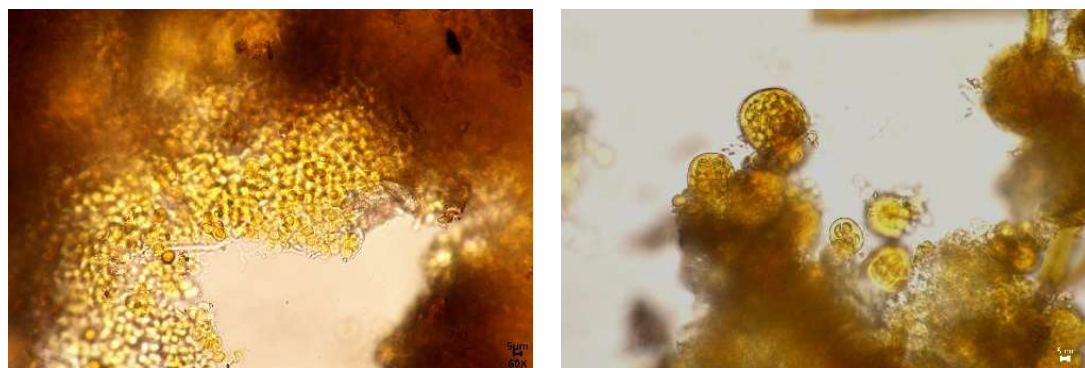
292

Fig. 5. Relative biomass percentage of marble surface of the Altar of Prayer for Good Harvest

293

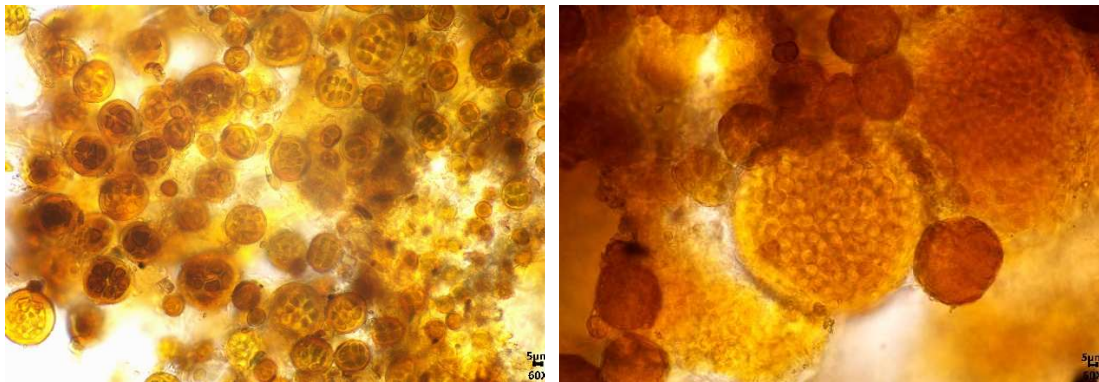
in the Temple of Heaven, Beijing, China.

294



a. *Myxosarcina* sp.

b. *Gomphosphaeria* sp.



c. *Asterocapsa* sp.

d. *Gloeocapsa* sp.1

295 **Fig. 6.** Dominant organisms on the marble surface of the altar of Prayer for Good Harvest
 296 in the Temple of Heaven, Beijing., China.
 297

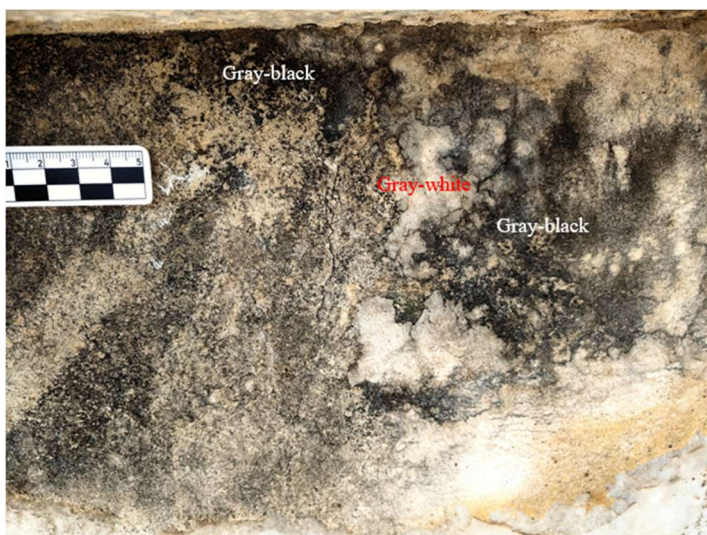
298 3.2 Characteristics of the distribution of biological communities on marble surfaces with
 299 different orientations in the study area

300 The Altar of Prayer for Good Harvests at the Temple of Heaven is a circular building (Fig. 16).
 301 The marble surfaces facing different directions receive varying amounts of sunlight. The south-
 302 facing surface receives the most sunlight, followed by the east and west-facing surfaces, which
 303 receive sunlight for half a day. The north-facing surface is shaded and receives no direct sunlight.
 304 This variation in sunlight exposure leads to differences in the biological populations on the rock
 305 surfaces. The details are discussed below:

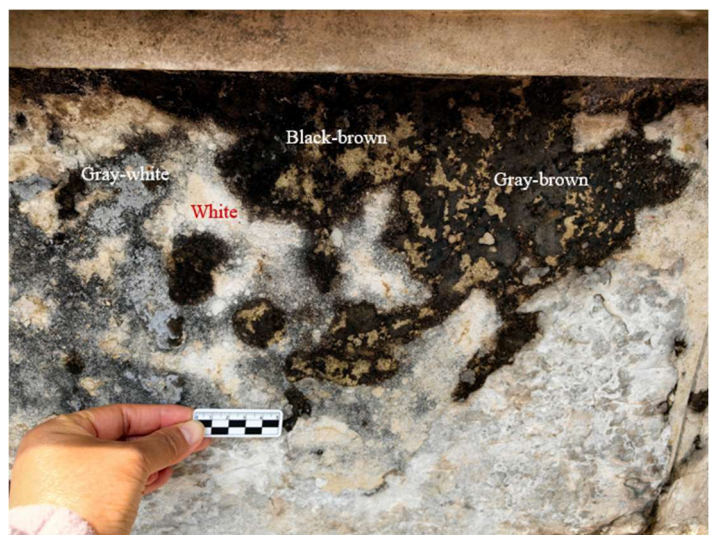
306
 307 3.2.1 Characteristics of Biological communities on East-Facing Rock Surfaces

308 The biological communities on east-facing rock surfaces are primarily characterized by gray-
 309 white, gray-brown, brown, gray-black, black-brown, white, and black-brown leathery appearances.
 310 The main species include *Scytonema* sp.2, *Chlorococcum* sp., *Gloeocapsa* sp.2, *Gloeothece* sp.1,
 311 *Myxosarcina* sp., *Phormidium* sp., *Calothrix* sp., *Gloeothece* sp.2, *Lyngbya* sp., *Gloeocapsa* sp.5,
 312 and *Chroococcus* sp.1 (Fig.7) . Among these, the dominant species are *Scytonema* sp.2,
 313 *Chlorococcum* sp., accounting for 25% and 23% of the relative biomass percentage (Fig. 8) .

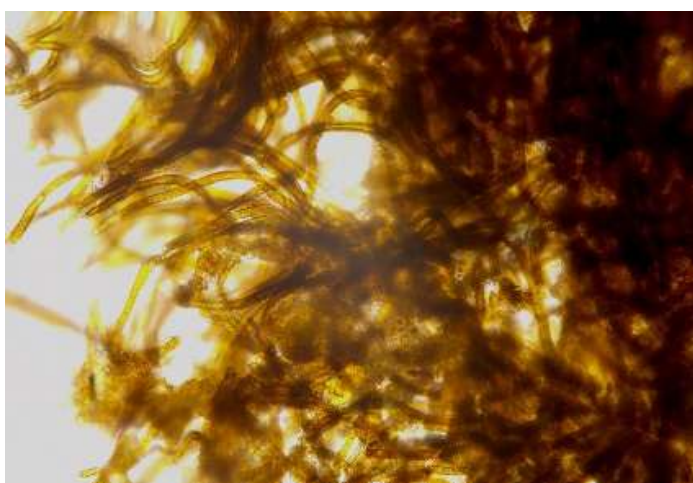
314
 315



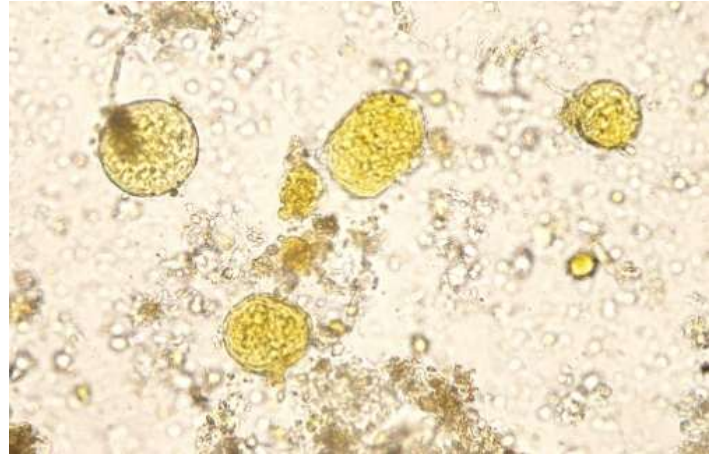
a. Gray-white, Gray-black



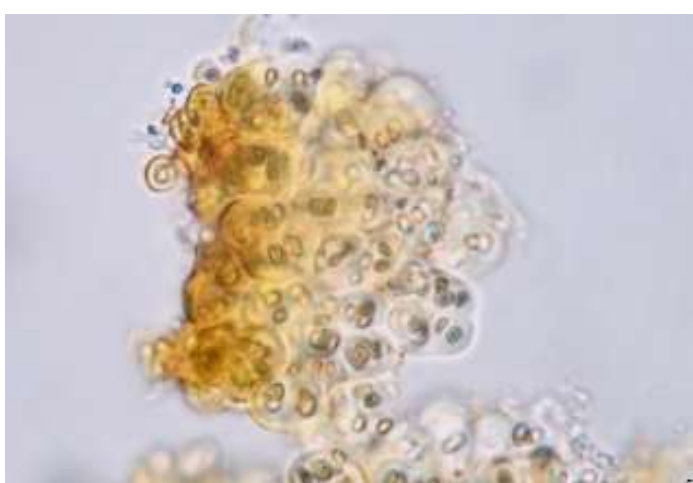
b. Gray-white, Gray-brown, Black-brown, White



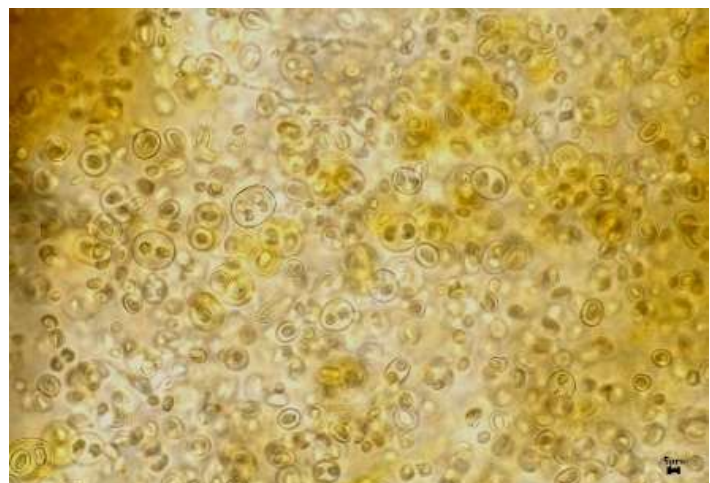
c. *Scytonema* sp.2



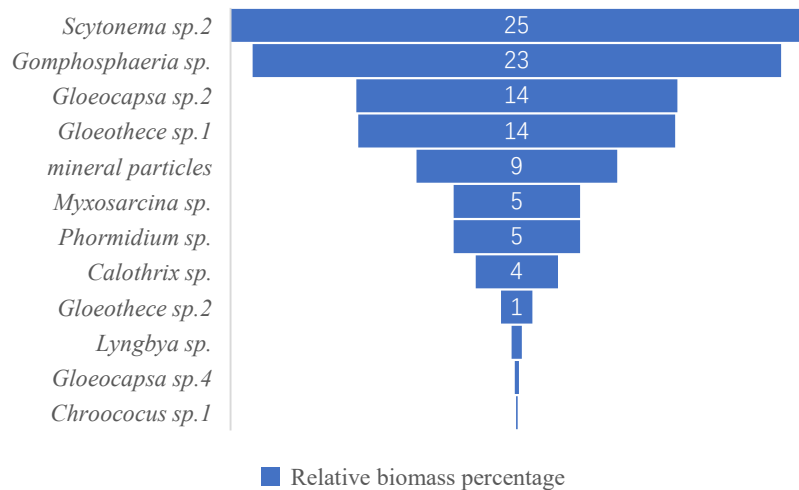
d. *Gomphosphaeria* sp.



e. *Gloeocapsa* sp.2



f. *Gloeothecae* sp.1



318

319

Fig.8. Biological population relative biomass percentage on the east-facing marble surface of the altar of

320

Prayer for Good Harvest in the Temple of Heaven, Beijing, China.

321

322 3.2.2 Characteristics of Biological communities on West-facing Rock Surfaces

323

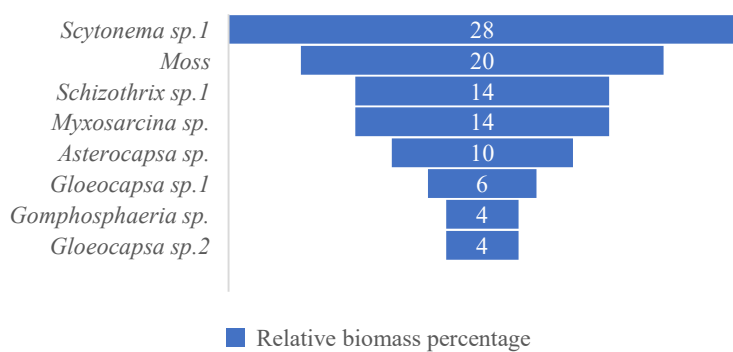
The biological communities on west-facing rock surfaces are primarily characterized by black hairy, black membranous, yellow-green leathery, gray-black leathery, yellow-green, brown, and gray-green appearances. The main species include *Scytonema* sp.1, mosses, *Schizothrix* sp.1, *Myxosarcina* sp., *Asterocapsa* sp., *Gloeocapsa* sp.1, *Gomphosphaeria* sp., and *Gloeocapsa* sp.2 et al (Fig. 9) . Among these, the dominant species are *Scytonema* sp.1 and mosses et al, accounting for 28% and 20% of the relative biomass percentage respectively (Fig. 10) .

329





330 **Fig. 9.** Micrographs of biomes and some species on the west-facing marble surface of the altar of
331 Prayer for Good Harvest in the Temple of Heaven, Beijing, China.
332



333
334
335 **Fig. 10.** Biological population relative biomass percentage on the west facing marble surface of the altar of
336 Prayer for Good Harvest in the Temple of Heaven, Beijing, China

337 3.2.3 Characteristics of communities Distribution on North-facing Surfaces

338 The biological communities on north-facing rock surfaces are primarily characterized by gray-
339 brown membranous, brown, gray-black, yellow-green, black-brown, gray-white, brown crusty,
340 brown carpet-like, brown-black leathery, and brown-black membranous appearances. The main
341 species include *Myxosarcina* sp., *Gomphosphaeria* sp., *Gloeocapsa* sp.1, *Schizothrix* sp.1,
342 *Asterocapsa* sp., *Scytonema* sp.1, *Calothrix* sp., mosses, *Gloeocapsa* sp.2, *Microcoleus* sp.,
343 *Chroococcus* sp., *Gloeothecae* sp.1, *Lyngbya* sp., *Gloeocapsa* sp., *Scytonema* sp.2, and *Synechocystis*
344 sp. et al (Fig. 11) . Among these, the dominant species are *Myxosarcina* sp. and *Gomphosphaeria*
345 sp., accounting for 17% and 15% of the relative biomass percentage respectively (Fig. 12) .

346

347



a. Gray-brown membranous



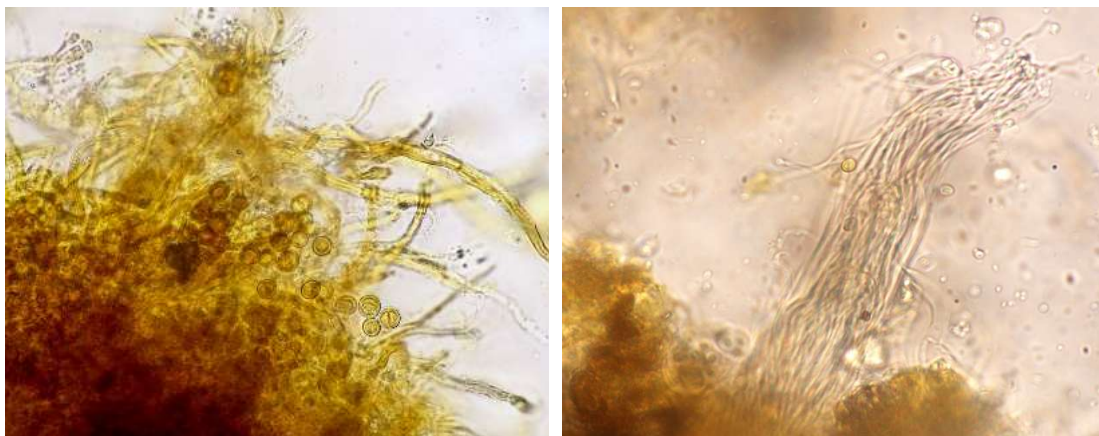
b. Gray-black



c. Yellow-green



d. Gray-white

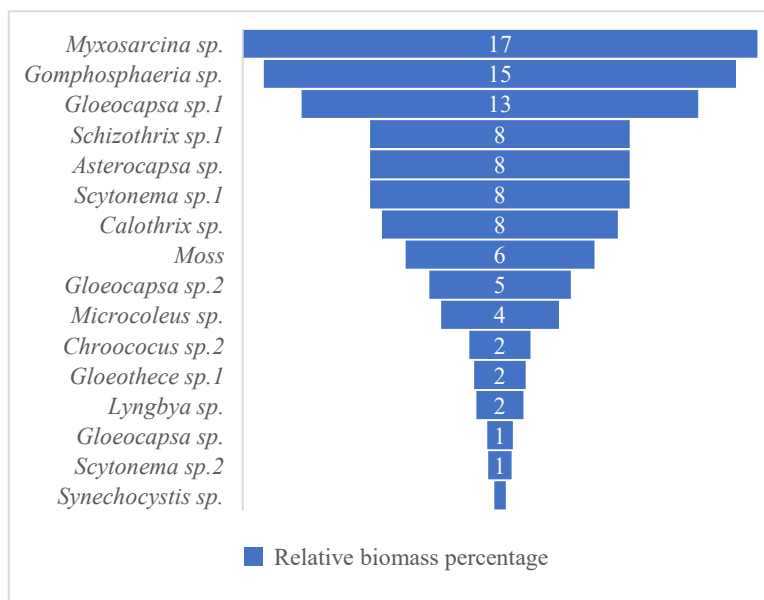


e. *Calothrix* sp.

f. *Microcoleus* sp.

348 **Fig. 11.** Micrograph of biological communities and some species on the north facing marble surface of the altar of
 349 Prayer for Good Harvest in the Temple of Heaven, Beijing, China.

350



351

352

353 **Fig. 12.** Relative biomass percentage of biological population on the north facing marble surface of the altar of
 354 Prayer for Good Harvest in the Temple of Heaven, Beijing, China.

355

356 3.2.4 Characteristics of communities Distribution on South-facing Surfaces

357 The biological communities on south-facing rock surfaces are primarily characterized by gray-
 358 green leathery, gray-white, gray-black membranous, black leathery, gray-black, brown-yellow, and
 359 green powdery layer appearances. The main species include *Scytonema* sp.1, *Nostoc* sp.,

360 *Asterocapsa* sp., *Myxosarcina* sp., *Phormidium* sp., *Gloeocapsa* sp.1, *Chroococcus* sp.1, *Schizothrix*
361 sp.4, *Microcoleus* sp., *Aphanocapsa* sp., *Chroococcus* sp.3, *Lyngbya* sp., *Gloeocapsa* sp.3, and
362 *Gloeocapsa* sp.4 et al (Fig. 14) . Among these, the dominant species are *Scytonema* sp.1 and *Nostoc*
363 sp., accounting for 25% and 20% of the relative biomass percentage respectively (Fig. 15) .



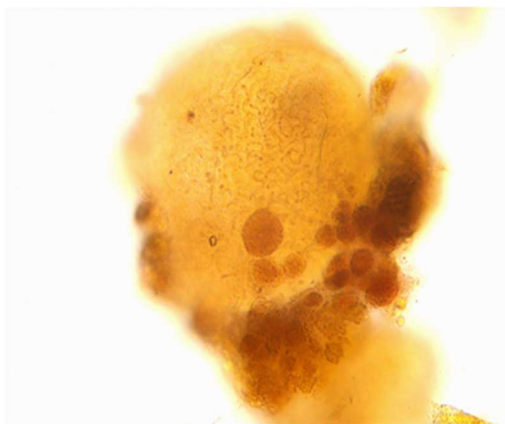
364 **Fig. 13.** Field photo of biomes on the south facing marble surface of the altar of
365 Prayer for Good Harvest in the Temple of Heaven, Beijing, China.
366
367



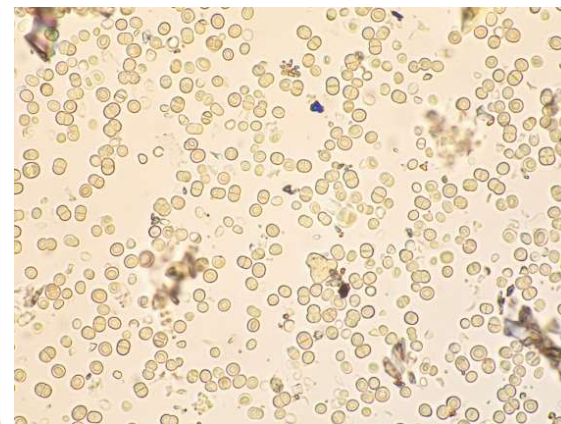
a. Green powdery layer magnified 60x



b. Green powdery layer magnified 400x



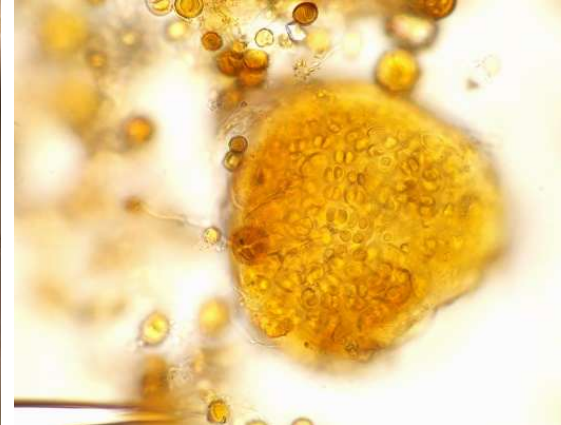
c. *Nostoc* sp.



d. *Chroococcus* sp.1



e. *Schizothrix* sp.3



f. *Chroococcus* sp.3

368

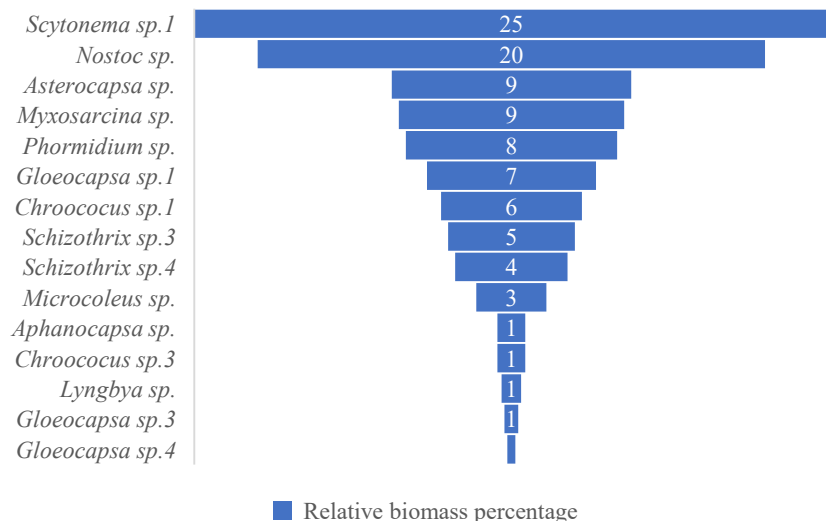
Fig. 14. Micrograph of biomes and some species on the south facing marble surface of the altar of

369

Prayer for Good Harvest in the Temple of Heaven, Beijing, China.

370

371



372

373

374 **Fig. 15.** Biological population relative biomass percentage on the south facing marble surface of the altar of
375 Prayer for Good Harvest in the Temple of Heaven, Beijing, China.

376

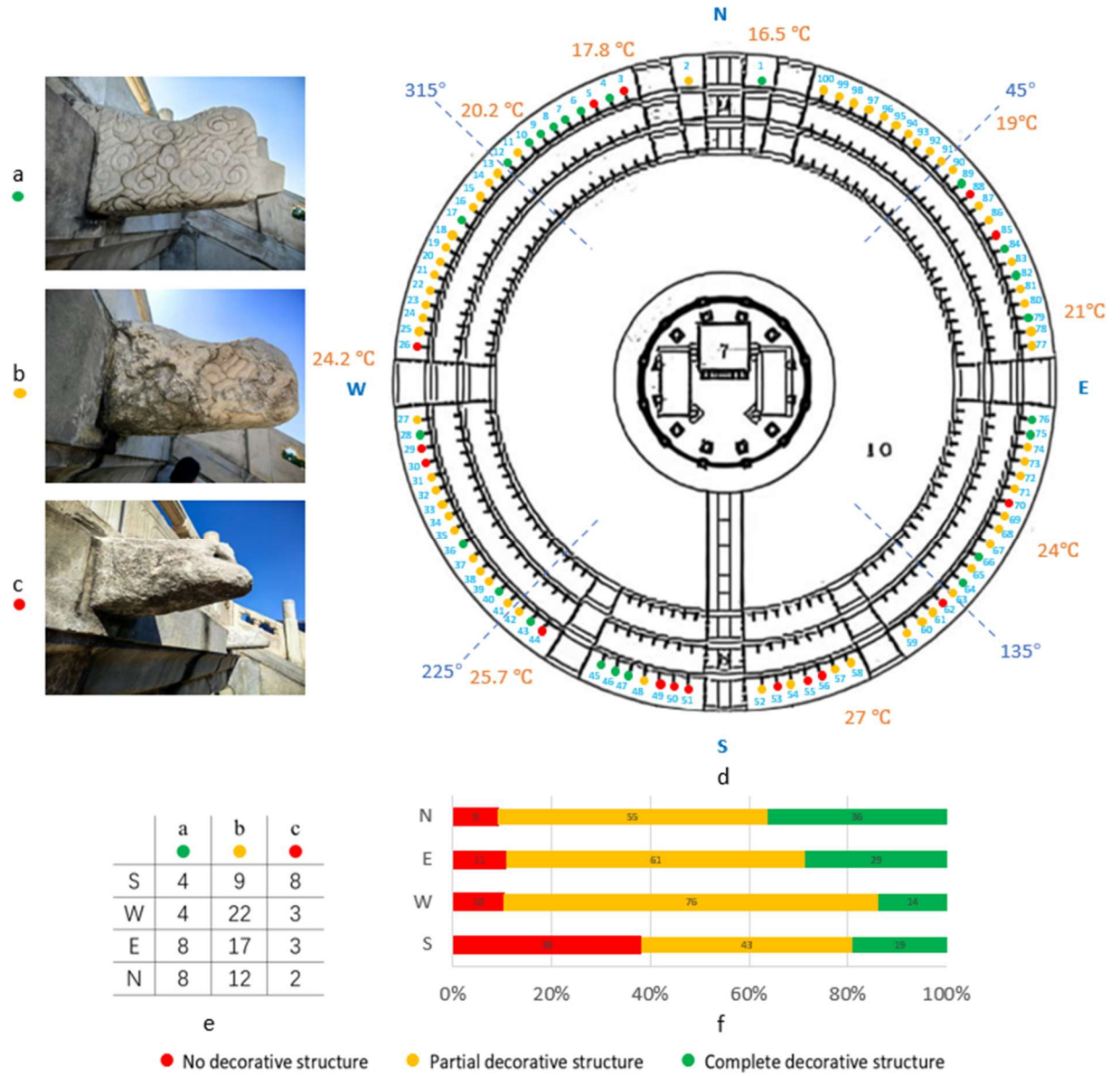
377 3.2.5 Comparison of communities on Different Orientations

378 The main aerial organisms on the rock surfaces include spherical cyanobacteria, small
379 filamentous cyanobacteria, and large filamentous cyanobacteria. Their distribution is primarily
380 influenced by the looseness of the substrate, sunlight, and moisture. From spherical cyanobacteria
381 to small filamentous cyanobacteria and then to large filamentous cyanobacteria, the requirement for
382 substrate looseness increases, the need for moisture decreases, and the requirement for sunlight
383 duration increases. Mosses, on the other hand, prefer shady and moist environments.

384 Although both the east and west-facing surfaces of the Altar of Prayer for Good Harvests in
385 the Temple of Heaven receive sunlight for half a day (Table 1), the east-facing surface receives
386 sunlight in the morning when the rock surface temperature is lower. Even with sufficient sunlight,
387 the growth of organisms on the east-facing surface is not as robust as on the west-facing surface.
388 The west-facing surface receives sunlight in the afternoon when the rock surface temperature is
389 higher, providing both water and heat conditions that are more favorable for biological growth. This
390 results in the presence of *Scytonema* sp.1, a cyanobacterium that prefers looser substrates, and more
391 mosses, leading to more severe weathering on the west-facing surface. The north-facing surface,
392 being in the shade, has slower evaporation rates and is mainly colonized by spherical cyanobacteria,

393 resulting in relatively weaker weathering. The south-facing surface receives more sunlight and
394 weathers faster, with the carved decorations on the rock surface completely destroyed (Fig. 13a).
395 The matrix is highly loose, and even large filamentous cyanobacteria like *Nostoc*, which typically
396 prefer to live in soil rather than on rock surfaces, are present. This indicates that the south-facing
397 marble has weathered severely, forming a loose, soil-like thick weathering layer. Additionally,
398 *Scytonema* sp.1, a species that thrives in sunny and dry environments and plays a significant role in
399 bioweathering, is also present. Mosses are not found on the south-facing side because they prefer
400 shady and moist environments. The orientation of the building, through differences in sunlight
401 duration and evaporation rates, creates a unique gradient of microhabitats, which in turn drives the
402 differential distribution of microbial communities and is accompanied by varying degrees of
403 weathering depending on the direction.

404 To further understand the environmental differences and weathering conditions of the rock
405 surfaces at the Altar of Prayer for Good Harvests in the Temple of Heaven, temperature
406 measurements were taken on a sunny afternoon in April (Fig. 16). The rock surface temperatures
407 were found to be highest in the southwest and lowest in the northwest. The Altar of Prayer for Good
408 Harvests was divided into four natural sectors, each centered on a cardinal direction and covering
409 45° to either side: North (N): 315°-45°, centered on true north, covering from northwest to northeast;
410 East (E): 45°-135°, centered on true east, covering from northeast to southeast; South (S): 135°-
411 225°, centered on true south, covering from southeast to southwest; West (W): 225°-315°, centered
412 on true west, covering from southwest to northwest. The weathering degree of 100 cloud dragon
413 heads on the third layer was statistically analyzed in each sector. The results showed that 40% of
414 the south-facing cloud dragon head decorations were completely weathered, indicating the most
415 severe weathering. The weathering degrees for the west, east, and north sectors decreased in that
416 order. This pattern is consistent with the distribution of biological organisms on the rock surfaces,
417 as shown in Table 1. The analysis of the weathering degree of 100 cloud dragon heads on the third
418 layer showed that 40% of the south-facing cloud dragon head decorations were completely
419 weathered, indicating the most severe weathering. The weathering degrees for the west, east, and
420 north directions decreased in that order. This pattern is consistent with the differences in weathering
421 in different directions revealed by the distribution of biological organisms on the rock surfaces
422 (Table 1).



423

424 Fig. 16 Rock surface temperatures and weathering conditions of the cloud dragon heads on the third layer of
425 the Altar of Prayer for Good Harvests at the Temple of Heaven in Beijing, China, on a sunny afternoon in April.

426 a: Cloud dragon heads with complete decorative structures.

427 b: Cloud dragon heads with partially weathered decorative structures.

428 c: Cloud dragon heads with completely weathered decorative structures.

429 d: A top-down simplified diagram of the Altar of Prayer for Good Harvests. The altar is divided into three layers, with 100 dragon
430 heads arranged along the edge of each layer. The dragon heads exhibit different degrees of weathering: red indicates completely weathered
431 decorative structures, yellow indicates partially weathered decorative structures, and green indicates intact decorative structures.

432 e: Statistical count of the number of cloud dragon heads with three different weathering degrees in four directions.

433 f: Calculation of the proportion of the three different weathering degrees of cloud dragon heads in different directions, revealing that

434 the weathering intensity of the dragon heads is highest in the south, followed by the west, east, and north.

435

436 **Table 1**

437 Environmental characteristics and dominant species of marble surface of the Altar of Prayer for Good
438 Harvests at the Temple of Heaven in Beijing, China.

439

Marble Surface Orientation	Sunlight	Moisture	Environmental Characteristics	Dominant Species	Weathering degree
North-facing	None	Slow evaporation	Cold and humid	Spherical cyanobacteria	
East-facing	Half day	Rapid evaporation in the morning	Warm and humid	Small filamentous cyanobacteria, Spherical cyanobacteria	Weak
West-facing	Half day	Rapid evaporation in the afternoon	Hot and humid	Small filamentous cyanobacteria, Mosses	
South-facing	Full day	Rapid evaporation during the day	Hot and dry	Small filamentous cyanobacteria, Large filamentous cyanobacteria	Strong

440

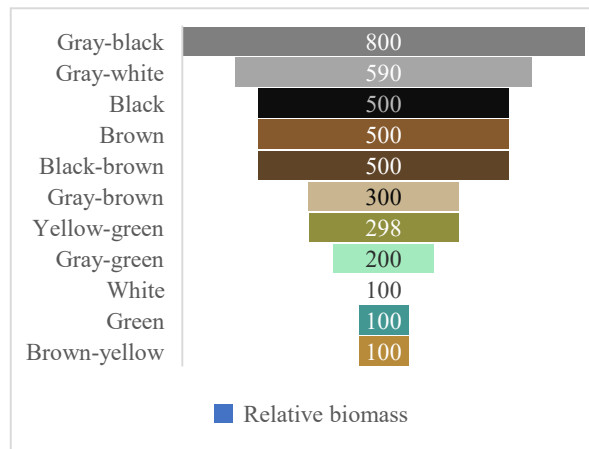
441 **3.3 Relative Biomass of Different Colored Biological Communities on Rock Surfaces in the Study**

442 **Area**

443 The colors displayed by organisms on rock surfaces differ from those observed under a
444 microscope. In this paper, the former is referred to as the "visual color," while the latter is called the
445 "microscopic color." The visual color is the community color presented when different populations
446 aggregate together, whereas the microscopic color is the color of different species observed under
447 magnification through a microscope. Often, communities of cyanobacteria with different
448 microscopic colors appear mostly black or gray-black of visual color.

449 The visual colors of biological communities on rock surfaces in the study area can be

450 categorized into gray-black, gray-white, black, brown, black-brown, gray-brown, yellow-green,
 451 gray-green, white, green, and brown-yellow. Their relative biomass is shown (Fig. 17) . The most
 452 common color is gray-black, followed by gray-white, black, brown, and black-brown. These are
 453 also typical colors exhibited by aerial cyanobacteria in the field, sometimes referred to as "ink
 454 bands." For example, the Nine Horses Fresco Hill (Jiuma Huashan) in the Guilin landscape of China
 455 is formed due to aerial cyanobacteria growing on the rocks, creating black ink-like bands.



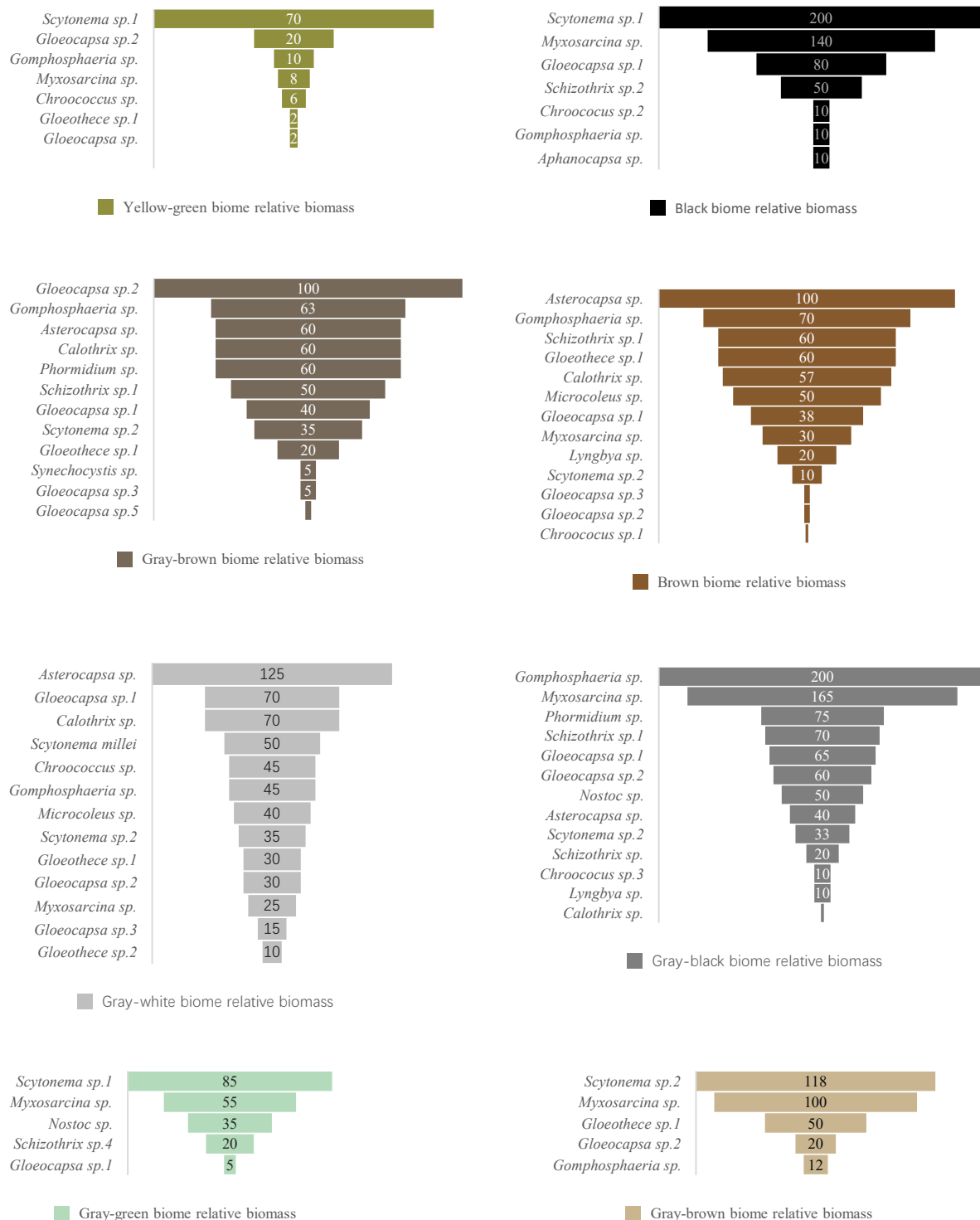
456
 457 **Fig. 17** Relative biomass of biomes with different colors on the marble surface of the Altar of Prayer for Good
 458 Harvests at the Temple of Heaven in Beijing, China.

459
 460 3.4 Relative biomass of communities' composition in different colored biological communities on
 461 rock surfaces in the study area

462 The relative biomass of different visual color biotic communities on the rock surface in the
 463 study area is shown (Fig. 18). An analysis of the main population compositions of these biological
 464 communities is presented (Fig. 19). The colors of biological communities on rock surfaces in the
 465 study area are primarily composed of black, brown, gray, green, and yellow, as well as combinations
 466 of these colors (gray-black, gray-white, black-brown, gray-brown, yellow-green, gray-green, and
 467 brown-yellow). The correlation between color combinations and population composition is not very
 468 apparent, which also indicates that determining microscopic color (population composition) through
 469 visual color is a complex and difficult task. Nevertheless, some patterns can be observed: Species
 470 like *Scytonema* sp.1, *Myxosarcina* sp., *Asterocapsa* sp., *Gomphosphaeria* sp., and *Gloeocapsa* sp.2
 471 tend to make the community color darker, presenting as black, brown, gray, or combinations of these;
 472 The parts that have a visual color of white are minerals, not biological organisms, under microscopic

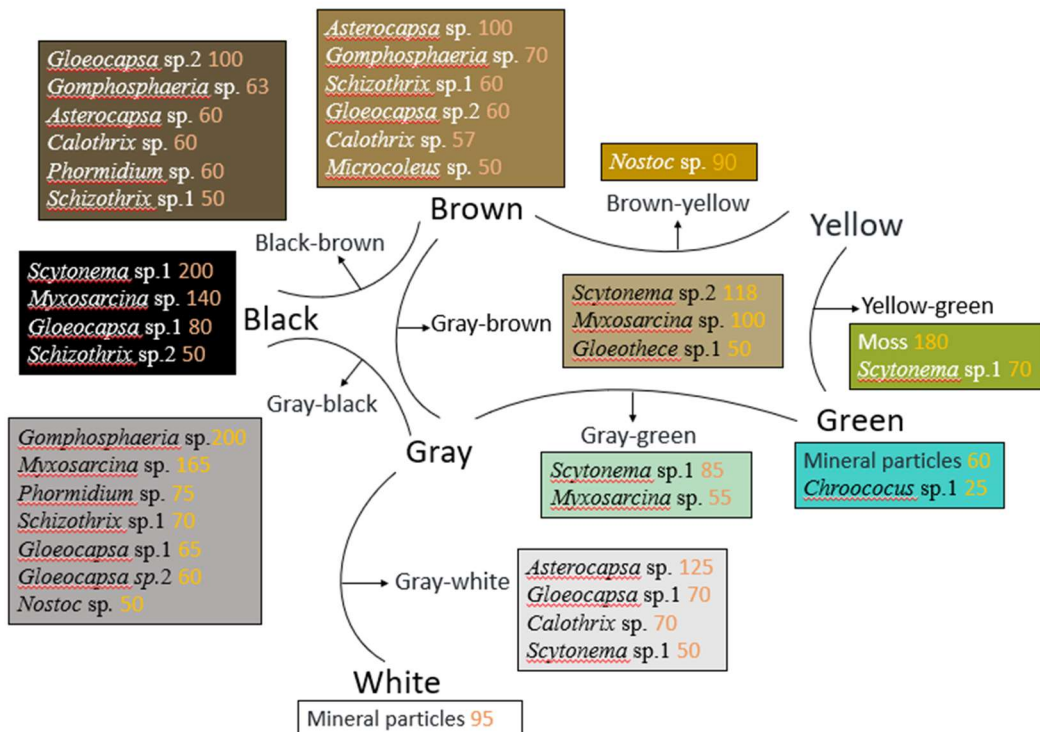
473 observation; the areas with a visual color of green (mainly referring to the characteristic blue-green
 474 of cyanobacteria) are mineral particles and *Chroococcus* sp.1; the areas with a visual color of
 475 yellow-green are mainly mosses; the areas with a visual color of brown-yellow are mainly *Nostoc*
 476 sp. etc.

477





478 **Fig. 18.** Relative biomass of community composition of different colors on marble surface of the Altar of Prayer
479 for Good Harvests at the Temple of Heaven in Beijing, China.
480

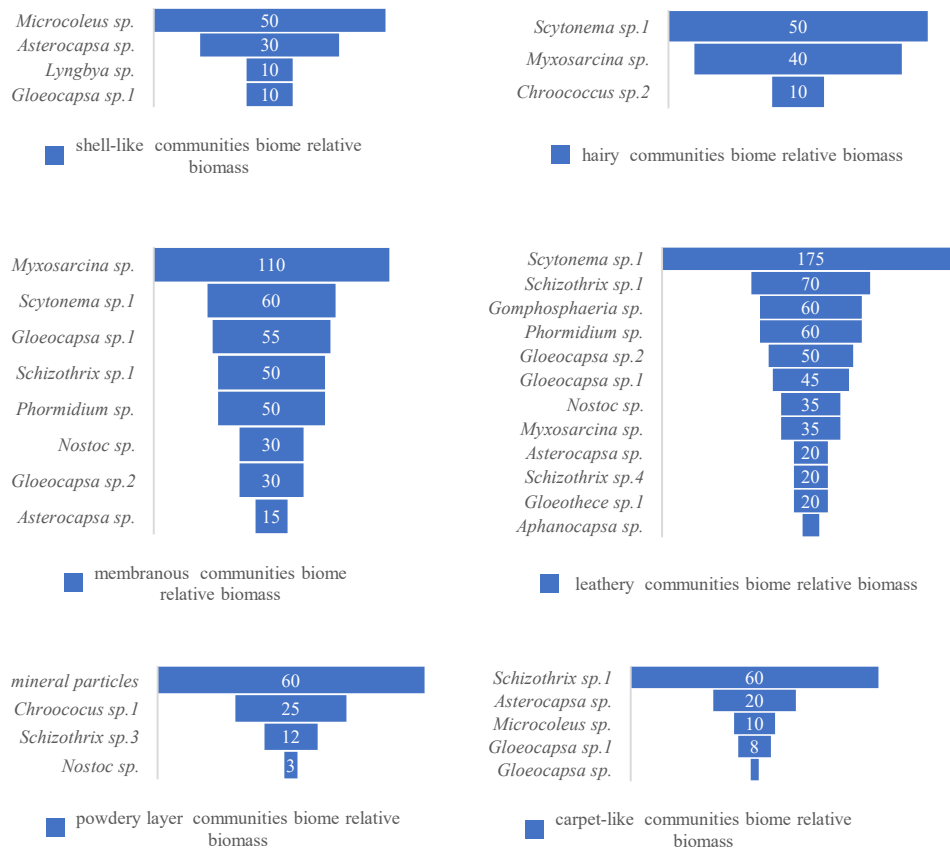


481
482 **Fig. 19.** Analysis of main population composition of different color biomes on marble surface of the Altar of
483 Prayer for Good Harvests at the Temple of Heaven in Beijing, China.
484

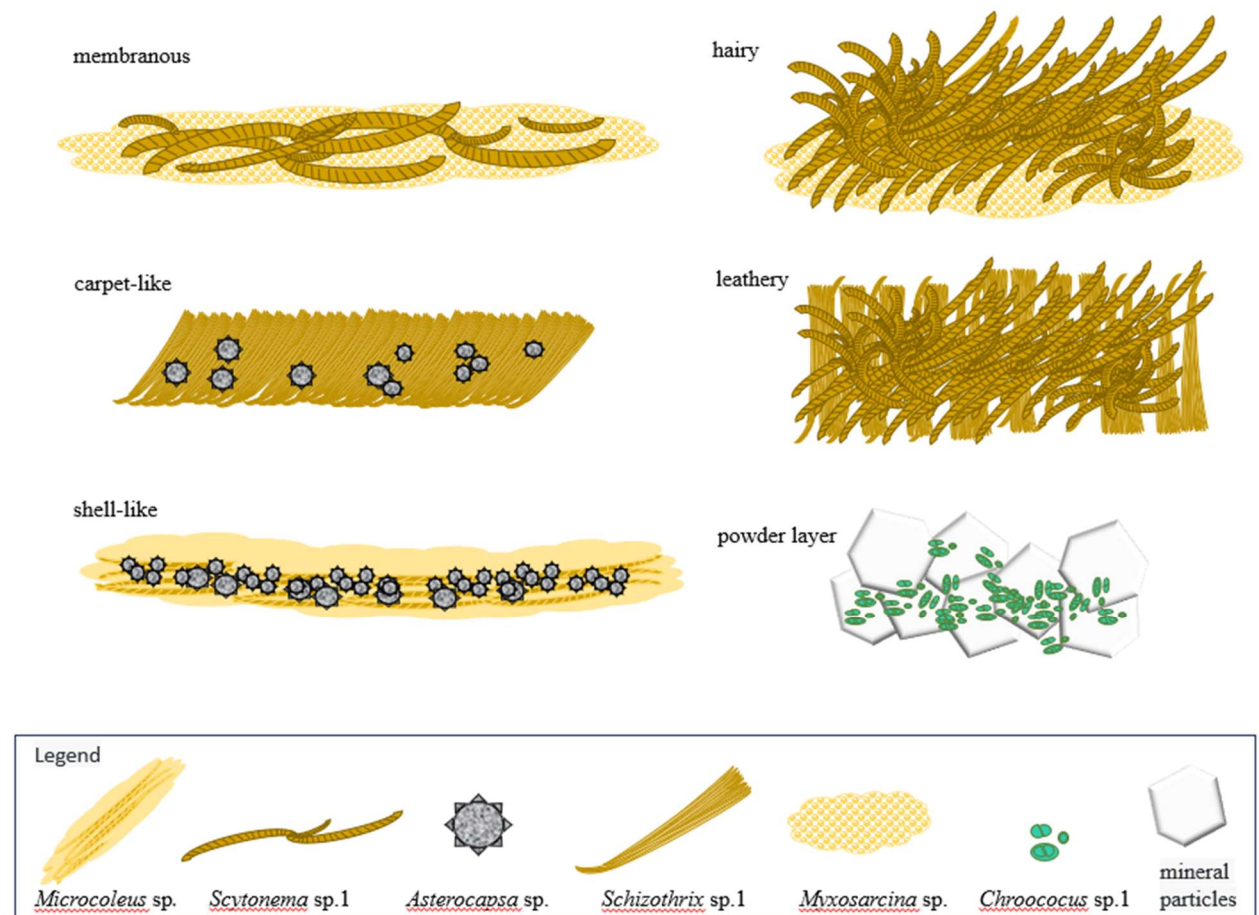
485 3.5 Relative biomass of communities composition in different morphological biological
486 communities on rock surfaces in the study area

487 The biological communities on rock surfaces in the study area exhibit different morphologies,
488 including membranous, hairy, carpet-like, leathery, shell-like, and powdery layers. Their relative

489 biomass of population composition is shown (Fig. 20). A diagrammatic explanation of the formation
 490 of these community morphologies is presented (Fig. 21).



491 **Fig. 20.** Relative biomass of different forms of community on marble surface of the Altar of Prayer for Good
 492 Harvests at the Temple of Heaven in Beijing, China.
 493



494

495 Fig. 21 Morphological genesis diagram of different communities on marble surface of the Altar of Prayer for Good

496

496 Harvests at the Temple of Heaven, China.

497

498 The dominant species in the membranous biological communities are mainly *Myxosarcina* sp.

499 and *Scytonema* sp.1. The former accounts for a relative biomass of 110, while the latter accounts for

500 60 (Fig. 17) . *Myxosarcina* sp. is spherical cyanobacteria (Fig.4a). It has thick individual sheaths,

501 forming a dense colonial mucilage. *Scytonema* sp.1 grows interspersed within, forming a

502 membrane-like community (Fig.21). When the relative biomass of *Scytonema* sp.1 in the

503 community exceeds that of *Myxosarcina* sp., it forms a hairy community (Fig.21). The dominant

504 species in the carpet-like communities are mainly *Schizothrix* sp.1 and *Asterocapsa* sp.. The former

505 accounts for a relative biomass of 60, while the latter accounts for 20 (Fig.20). *Schizothrix* sp.1

506 grows densely together, forming a carpet-like structure (Fig. 21). The dominant species in the

507 leathery biological communities are mainly *Scytonema* sp.1 and *Schizothrix* sp.1. The former

508 accounts for a relative biomass of 175, while the latter accounts for 70 (Fig. 20). *Scytonema* sp.1

509 intertwines, with *Schizothrix* sp.1 interspersed within (Fig. 21). The dominant species in the shell-
510 like biological communities are mainly *Microcoleus* sp. and *Asterocapsa* sp.. The former accounts
511 for a relative biomass of 50, while the latter accounts for 30 (Fig.20). *Microcoleus* sp. has well-
512 developed sheaths, with multiple algal filaments inside each sheath. The sheaths of multiple
513 *Microcoleus* sp. aggregate to form a mucilaginous layer, with *Asterocapsa* sp.1 dispersed within.
514 When the mucilaginous layer dries, it cracks into numerous small pieces. The edges of each piece
515 detach from the rock surface and curl up, forming a shell-like structure (Fig. 21 and Fig. 22) . The
516 powder layer is a severely weathered surface (Fig. 13d). Under microscopic observation, it mainly
517 consists of mineral particles and *Chroococcus* sp.1, with the former accounting for 60 and the latter
518 for 20 of the relative quantity (Fig. 20). *Chroococcus* sp.1 is distributed on the surface and in the
519 crevices of mineral particles (Fig. 14a and b). The color of the community appears as a mixture of
520 the green color of *Chroococcus* sp.1 (or the blue-green color characteristic of cyanobacteria) and the
521 white color of mineral particles.

522

523 3.6 Bioweoathering on Rock Surfaces in the Study Area

524 The growth distribution of aerial organisms on rock surfaces in the study area is closely related
525 to the surface smoothness and texture of marble (Table 2). If the marble surface is uneven or has a
526 non-uniform texture, the aerial organisms' communities will be distributed in a spotted pattern (Fig.
527 22a). Dissolution forms solution pits and cavities (Fig. 22b), which further expand into solution
528 basins (Fig. 22c, d). If the marble surface has linear textures or non-uniform texture with joint stripes,
529 the aerial organisms' communities will be distributed in a linear pattern (Fig. 22e). Dissolution forms
530 solution marks and grooves (Fig.22f), which further expand into solution channels (Fig. 22g). If the
531 marble surface is smooth and has a uniform texture, the aerial organisms' communities will be
532 distributed in a planar pattern (Fig. 22h). Dissolution forms a weathering layer or spalling layer (Fig.
533 22i).

534

535 **Table 2**

536 Characteristics of the Marble Surface of the Altar of Prayer for Good Harvests in the Temple of
537 Heaven, Beijing, China, and the Process of Biological Erosion on Its Surface.

Marble Characteristics	Biological Community	Resulting Dissolution	Development
	Distribution	Forms	Process
Uneven surface or non-uniform texture	Spotted distribution	Solution pits, cavities, and basins	
Surface with linear textures or non-uniform texture with joint stripes	Linear distribution	Solution marks, grooves, and channels	
Smooth surface with uniform texture	Areal distribution	Weathering layer, spalling layer	

538

539

540

541



a. biological community point distribution



b. Solution pores and solution cavities



c. Sinkhole





542 **Fig. 22** Bioweathering forms on the marble surface of the Altar of Prayer for Good Harvests in the Temple of
 543 Heaven, Beijing, China.

544

545

546 The spotted distribution of biological communities gradually expands into linear distribution,
 547 and then into areal distribution. Solution pits, basins, and cavities also further enlarge their
 548 dissolution forms, developing into solution marks, grooves, and channels. For example, in the study

549 area, the weathering process of white marble “cloud Chi Head” begins with the accumulation and
550 growth of organisms in the low-lying areas of the cloud patterns (Figures 23a, b).. These areas retain
551 more moisture, so they are the first to undergo bioweathering, forming deeper solution cavities and
552 channels. The communities then gradually spread to the surrounding areas, developing into linear
553 distributions, and then areal distributions, leading to flaking of the rock surface (Fig. 23c). This
554 partially destroys the pattern structure, further expanding the area and depth of dissolution, forming
555 a loose powder layer (Fig. 13a, d; Fig. 14a, b; Fig. 16b, c; Fig. 23d, e).

556



a. The organisms gather and grow in the low-lying areas of the cloud chi head ornamentation.



b. The organisms gather and grow in the low-lying areas of the cloud chi head ornamentation.



c. The surface of the cloud chi head is flaking off in patches.



d. The cloud chi heads have even weathered away completely.



e. A loose, powdery layer has formed on the surface of the cloud chi heads, with a large amount of cyanobacteria growing inside.

557

Fig. 23. Bioweathering process of the cloud Chi Head on the Altar of Prayer for Good Harvests in the Temple of

558 Heaven, Beijing, China.

559

560 **4 Discussion**

561 (1) This study focuses on the cyanobacterial and bryophyte communities that can be observed
562 using biological microscopy. The current scope of the research has not yet covered other microbial
563 groups. To determine whether other bacterial groups exist on the surface of stone cultural relics and
564 to understand their ecological functions, further systematic verification through subsequent studies
565 is still needed. At the methodological level for the classification and identification of cyanobacteria,
566 traditional morphological identification, although it may lead to taxonomic deviations at the genus
567 and species levels, molecular biology methods also face technical bottlenecks. For special samples
568 like biofilms on stone cultural relics, molecular testing typically requires microbial samples with a
569 high purity of more than 0.2 grams. However, in actual sampling, due to restrictions on cultural relic
570 protection, sometimes only trace amounts of less than 0.01 grams can be obtained. While such low
571 sample quantities are sufficient for morphological identification under a biological microscope, they
572 pose significant challenges for molecular biology methods. Low DNA extraction efficiency and
573 significant amplification bias from such small samples can result in decreased taxonomic resolution.
574 Furthermore, there has been long-standing controversy in the taxonomy of cyanobacteria. The
575 conflict between traditional morphological classification and molecular systematics has led to a
576 dynamic revision of the taxonomic framework. This instability makes it difficult to match taxonomic
577 information when annotating environmental samples using 16S rRNA gene sequence databases
578 (Lefler, et al., 2023). Future research should aim to construct a multidimensional identification
579 system, integrating microscopic observation, culturomics, and metagenomics, to gradually establish
580 classification standards and databases suitable for the study of microorganisms in cultural heritage.
581 This will be an important direction for the development of methodologies in this field.

582 (2) The differential weathering characteristics of the cloud chi heads on the Altar of Prayer for
583 Good Harvests, as well as the directional differences in the spatial distribution of organisms on the
584 rock surface, show significant consistency. This correspondence confirms the scientific validity of
585 the visual analysis method based on the relative volume and the relative volume percentage
586 determined by microscopic observation. This method, through the analysis of micro-scale biotic
587 community features, can effectively reflect the differences in weathering processes in the macro-

588 environment, providing an important reference for establishing the correlation between micro-
589 observation indicators and macro-environmental factors.

590 (3) The bioweathering process of the marble at the Altar of Prayer for Good Harvest in the
591 Temple of Heaven is controlled by both macro-hydrological dynamics and micro-surface
592 topography: On a macro scale, in areas with low flow during heavy rain (raised areas), water quickly
593 drains away, resulting in sparse biofilms and weak bioweathering. In high-flow areas during heavy
594 rain (water-collecting grooves), the extended water retention time leads to the formation of "ink
595 bands" rich in cyanobacteria, resulting in strong bioweathering. On a micro scale, the micro-
596 topographic features of the rock determine the colonization patterns of organisms by regulating local
597 hydrological conditions—irregular rough surfaces induce point-like biological aggregation due to
598 discrete water films, leading to the development of solution pores and pits; linear decorations or
599 joint surfaces promote linear biological expansion due to directional water storage, forming solution
600 marks and grooves; smooth and dense surfaces support planar biological growth due to uniform
601 water film coverage, ultimately leading to the overall peeling of the weathered layer. This coupled
602 mechanism reveals that, in addition to the different sunlight exposure on the rock surface caused by
603 orientation, the synergistic regulation of spatiotemporal water distribution and rock surface
604 characteristics is also an important reason for the different distribution of biological communities
605 on stone cultural relics. Some studies also suggest that the type of stone, its position on the building,
606 and the surface roughness of the stone greatly influence biological growth (Korkanç and Savran,
607 2015). Some organisms (such as cyanobacteria and lichens) also bore into the marble, forming a
608 hard, black, porous layer (Golubić, et al., 2015). The biological black crust on marble is often
609 attributed to physical and inorganic chemical causes such as dust, which needs to be taken seriously.

610 (4) The connections and issues between different research levels, methods, and results in this
611 paper.

612 Connections and issues between different research levels, methods, and results in this paper.
613 This paper studies the aerial organisms on rock surfaces in the research area in terms of biological
614 community population composition, community color and morphology, and community distribution
615 characteristics (Table 3). The spotted, linear, and planar distributions of biological communities on
616 rock surfaces in the study area are composed of many microcommunities. These microcommunities
617 exhibit different morphologies, including membranous, hairy, carpet-like, leathery, shell-like, and

618 powder layers. Spotted, linear, and areal distributions of biological communities may be composed
619 of one type of microcommunity or multiple types. Microcommunities are further composed of
620 multiple populations, and a population consists of multiple individual organisms of the same species.

621 Community distribution characteristics are observed with the naked eye, without
622 magnification. Community color and shape are observed through stereomicroscopes and the naked
623 eye, magnifying objects 8-56 times (or no magnification if observed with the naked eye). Biological
624 community population composition is identified through biological microscope observation,
625 magnifying objects 40-1000 times. This represents three stages of research with increasing
626 magnification of the research object: 1) Distribution area; 2) Community; 3) Population. Research
627 at each stage is relatively easy to conduct, but the connections between stages are challenging and
628 represent a key focus of this paper. For example, to accurately correlate different colored and shaped
629 communities with their precise population compositions (i.e., connecting the community stage with
630 the population stage) requires statistical analysis of numerous specimens to improve accuracy.
631 Additionally, for outdoor observations of communities, which involve the transition between the
632 distribution area stage and the community stage, the primary method is still visual observation with
633 the naked eye. Only a small number of observations are conducted using stereomicroscopes because
634 detailed stereomicroscopic observations that require photography must be done indoors. Sampling
635 of cultural relics in scenic areas is extremely limited and must be carried out without damaging the
636 relics. To address this issue, one approach is to enhance the performance of observation equipment
637 to allow for in situ biological community observations outdoors without sampling, or to perform
638 minimal sampling.

639 **Table 3**

640 Analysis of Research Levels in the Study on aerial organisms on marble of the Altar of Prayer for Good Harvests
641 in the Temple of Heaven, Beijing, China.

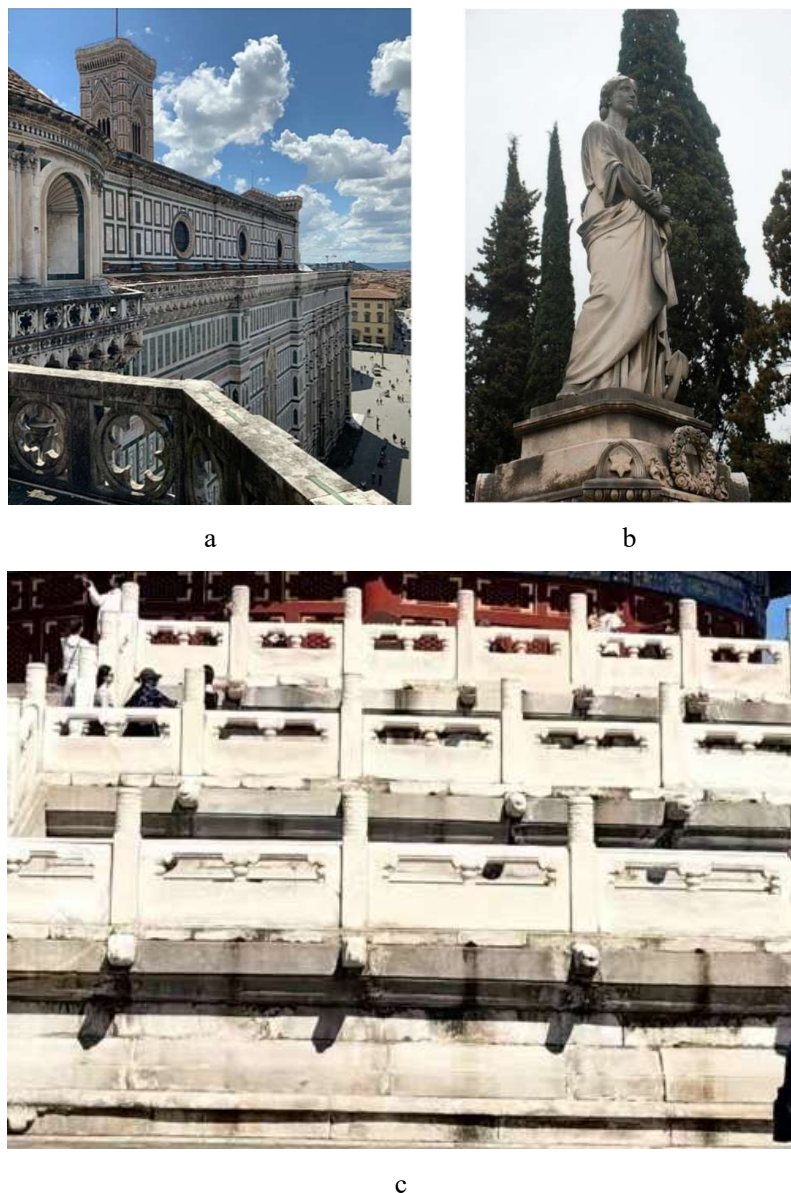
Research Level	Distribution Area	Community	Population
Observation Method	Naked eye	Stereomicroscope, naked eye	Biological microscope
Magnification	0	8-56, 0	40-1000
Classification	3 distribution characteristics (point, linear, and areal)	11 colors:	30 genera and species :

distribution)	gray-black, gray-white, black, brown, black-brown, gray-brown, yellow-green, gray-green, white, green, brown-yellow 6 morphologies: membranous, hairy, carpet- like, leathery, shell-like, and powder layer	<i>Myxosarcina</i> sp., <i>Gomphosphaeria</i> sp., <i>Asterocapsa</i> sp. and so on (Fig.5)	
Composition	Composed of multiple communities	Composed of multiple populations	Composed of multiple individuals of a single species

642

643 (5) In this study, the weathering intensity of the Altar of Prayer for Good Harvests in the Temple of
 644 Heaven is found to be south-facing > west-facing > east-facing > north-facing. Additionally, the
 645 metabolic activity of the southeastern microbial community on the marble of Florence Cathedral is
 646 higher than that of the northwestern community (Checcucci, et al., 2022). This indicates that the
 647 weathering of stone cultural relics exhibits directional differences, and these directional differences
 648 vary in different climate zones. When studying the microenvironment of rock surfaces, temperature
 649 is relatively easy to measure, but humidity is difficult to measure accurately due to the significant
 650 influence of wind disturbances, which can lead to measurement failures. Therefore, more effective
 651 methods are needed to address this issue. Another comparison can be made between the marble
 652 relics of the Cathedral of Santa Maria del Fiore in Florence, Italy, and the Speranza statue (the
 653 Cathedral of Santa Maria del Fiore was completed in 1887 and is 135 years old; the Speranza statue
 654 was built in 1863 and is 158 years old). The growth of black biofilm on these structures is
 655 significantly more extensive and faster than that on the Altar of Prayer for Good Harvests at the
 656 Temple of Heaven in Beijing (built in 1420 and 605 years old). The primary reason for this
 657 difference is the climate. Florence has a Mediterranean climate with high rainfall (about 850 mm)
 658 (Venturi et al., 2020), while Beijing has a temperate monsoon climate with low annual rainfall
 659 (During the period from 2009 to 2024, the multi-year average annual total rainfall was 610 mm,

660 according to data from the National Meteorological Science Data Center Website.). Therefore, water
661 is the primary factor determining the growth rate and distribution area of the black biofilm on marble.
662 Additionally, the different physical properties of marble in the two locations should also be
663 considered.



664 Fig. 24: Comparison of Black Biofilm Growth on Marble Relics in Florence and Beijing
665 a. Cathedral of Santa Maria del Fiore in Florence (façade completed in 1887, 138 years old, using white, green, and pink marble), with a
666 large area covered by black biofilm (Santo, 2023);
667 b. Speranza statue in Florence (built in 1863, 158 years old, using white marble), with a large area covered by black biofilm (Mascalchi,
668 2018);
669 c. Altar of Prayer for Good Harvests at the Temple of Heaven in Beijing (built in 1420, 605 years old, using white and bluish-white marble),

670 with a small area covered by black biofilm, mainly distributed in areas with high runoff from sudden rain.

671 (6) The species in the study area, such as *Scytonema* sp.2, are also common aerial cyanobacteria

672 found on limestone surfaces (Tian, et al., 2002; Tian, et al., 2003; Tian, et al., 2004). They prefer

673 calcareous environments, are drought-resistant, grow slowly, and have extremely strong vitality.

674 The mechanism of dissolve rocks primarily involves the biological need to obtain inorganic

675 nutrients such as calcium and magnesium ions from the rock. Aerial organisms can secrete organic

676 acids, which release calcium and magnesium ions from the rock, providing the inorganic nutrients

677 necessary for their growth and development. Through this acid dissolution process, aerial organisms

678 can "eat away" at the rock, forming small hemispherical dissolution pits. This process damages the

679 surface structure of the rock, leading to the formation of an underlying weathering layer (Tian, et

680 al., 2004). In addition, various forms of cyanobacterial communities in extremely arid environments,

681 such as on rocks, develop thicker exopolysaccharide (EPS) sheaths to retain intracellular water. The

682 EPS sheath undergoes contraction and expansion in response to changes in weather conditions,

683 accelerating the disintegration of rock particles on the surface of rocks. This process is very similar

684 to microbial weathering in the Atacama Desert (Jung, et al., 2020). Both processes involve the

685 swelling of the EPS due to water absorption, leading to the deformation of the biofilm and the

686 detachment of the rock surface at the community scale. This results in the expansion of patchy

687 weathering into a more extensive weathering layer (such as the Atacama terrestrial protopedon or

688 the powdery layer at the Temple of Heaven) at the landscape scale. The mechanism involves the

689 tensile stress generated by the swelling of the EPS exceeding the local tensile strength of the rock,

690 initiating cracks (such as grain boundary cracking in the Atacama and mineral particle detachment

691 at the Temple of Heaven). These cracks provide pathways for chemical and biological erosion,

692 leading to an expanded pore/crack network, increased water retention time, enhanced biological

693 activity, and further swelling, creating a self-reinforcing weathering loop. It is clear that the swelling

694 effect plays a crucial role as a "physical engine" in microbial bioweathering. Future research should

695 focus on cross-scale mechanical modeling: scaling up the swelling force of microbial EPS (at the

696 nN level) to the point of rock fracture (at the MPa level) to reveal the mechanisms of scale transition;

697 quantifying the impact of changes in fog/rain patterns under global warming on the frequency of

698 biological swelling, to warn of accelerated weathering risks; and recognizing that swelling not only

699 acts as a "trigger" for rock destruction but also serves as a key link between biological activity and

700 surface processes. Its universality across different environments provides a new perspective for
701 understanding the evolution of the Earth's critical zone.

702

703 5 Conclusion

704 (1) The most dominant species on marble surfaces in the study area is *Myxosarcina* sp., followed
705 by *Gomphosphaeria* sp., *Asterocapsa* sp.1, *Gloeocapsa* sp.1, and *Scytonema* sp.1. These
706 aerobic cyanobacteria prefer calcareous environments, are drought-tolerant, slow-growing, and
707 extremely resilient.

708 (2) The biological population composition on marble surfaces facing different directions of the
709 Altar of Prayer for Good Harvests in the Temple of Heaven varies due to differences in sunlight
710 exposure. The east-facing side, warm and humid, mainly hosts small filamentous and spherical
711 cyanobacteria such as *Scytonema* sp.2 and *Gomphosphaeria* sp. The west-facing side, hot and
712 humid, primarily features *Scytonema* sp.1 and mosses, with *Scytonema* sp.1 being small
713 filamentous cyanobacteria. The north-facing side, cold and humid, mainly supports spherical
714 cyanobacteria like *Myxosarcina* sp. and *Gomphosphaeria* sp. The south-facing side, hot and dry,
715 primarily hosts small or large filamentous cyanobacteria such as *Scytonema* sp.1 and *Nostoc*
716 sp.. The observed weathering intensity in different directions is: south > west > east > north,
717 which is entirely consistent with the varying degrees of weathering reflected by the cloud
718 dragon heads in each direction. This indicates that the visual analysis method based on the
719 relative volume and relative volume percentage of species, as determined by microscopic
720 observation and statistical analysis, is scientifically valid.

721 (3) Rock surface biological communities in the study area display various colors, with gray-black
722 being the most common, followed by gray-white, black, brown, and brown-black. Gray-black
723 communities are mainly composed of *Myxosarcina* sp. and *Gomphosphaeria* sp.

724 (4) Rock surface biological communities in the study area exhibit different morphologies, including
725 membranous, hairy, carpet-like, leathery, shell-like, and powder layers. Different morphologies
726 correspond to different population compositions.

727 (5) In addition to sunlight exposure, the growth of aerial organism on the rock surfaces in the study
728 area is also controlled by macro-hydrological dynamics and micro-surface topography. On a
729 macro scale, in areas with low flow during heavy rain, the biofilm is sparse, and the

730 bioweathering effect is weak. In areas with high-flow areas during heavy rain, "ink bands" rich
731 in cyanobacteria form, leading to strong bioweathering. On a micro scale, the microtopographic
732 features of the rock regulate local hydrological conditions, determining the colonization
733 patterns of the organisms: On uneven or heterogeneous marble surfaces, aerial organism
734 communities are distributed in patches, leading to the formation of solution pores, cavities, and
735 pits; On marble surfaces with linear patterns or heterogeneous textures with joint lines, aerial
736 organism communities are distributed in linear patterns, leading to the formation of solution
737 marks, grooves, and channels. On flat and homogeneous marble surfaces, aerial organism
738 communities are distributed in a planar pattern, leading to the formation of weathering layers
739 or spalling layers. The thicker exopolysaccharide (EPS) sheath of aerial cyanobacteria can
740 undergo contraction and expansion, thereby accelerating the disintegration of rock particles on
741 the surface of rocks. Preventing or reducing the growth of aerial organism is key to slowing
742 down the bioweathering process of the marble at the Altar of Prayer for Good Harvests in the
743 Temple of Heaven.

744

745 **Author contributions**

746 YT completed all the work on the paper, including sampling, photography, experimental data
747 analysis, charting, drawing, and writing the paper, among other tasks.

748

749 **Competing interests**

750 The author has declared that there are no competing interests.

751

752 **Acknowledgement**

753 This study was supported by National Science Foundation of China (Grant No. 40872197) and the
754 Development Fund of China University of Geosciences (Beijing) (Grant No. F02114).

755

756 **References**

757 Beijing Institute of Ancient Architecture.: Research and Application of Stone Structure Protection
758 in Ancient Buildings in Beijing. Beijing: China Literature and History Press. 1-330, 2018.
759 C. Gaylarde, C.: Influence of Environment on Microbial Colonization of Historic Stone Buildings

760 with Emphasis on Cyanobacteria. Heritage. 3. 1469-1482.
761 <https://doi.org/10.3390/heritage3040081>, 2020

762 Checcucci, A, Borruso, L, Petrocchi, D, Perito, B.: Diversity and metabolic profile of the microbial
763 communities inhabiting the darkened white marble of Florence Cathedral. International
764 Biodeterioration & Biodegradation, 171- . <https://doi.org/10.1016/j.ibiod.2022.105420>, 2022.

765 Danin, A., Caneva, G.: Deterioration of limestone walls in Jerusalem and marble monuments in
766 Rome caused by cyanobacteria and cyanophilous lichens. International Biodeterioration,
767 26(6): 397-417, [https://doi.org/10.1016/0265-3036\(90\)90004-Q](https://doi.org/10.1016/0265-3036(90)90004-Q), 1990

768 Desikachary, T. V.: Cyanophyta. Indian Council of Agricultural Research. New Delhi.1~669.
769 <https://doi.org/10.1086/403350>, 1959

770 Fott, B. (Translated by Luo,d.): Phycology. Shanghai: Shanghai Science and Technology Press. 11-
771 396, 1980.

772 Geitler, L.: Cyanophyceae. In L.Rabenhorst'S Kryptogamen-Flora, Band 14. Leipzig, Germany:
773 Akademische Verlagsgesellschaft m.b.H..1~1194, 1932.

774 Gioventù, E., Lorenzi, P. F., Villa, F., Sorlini, C., Rizzi, M., Cagnini, A., Griffo, A., Cappitelli, F.:
775 Comparing the bioremoval of black crusts on colored artistic lithotypes of the Cathedral of
776 Florence with chemical and laser treatment. International Biodeterioration & Biodegradation,
777 65(6): 832-839, <https://doi.org/10.1016/j.ibiod.2011.06.002>, 2011

778 Golubić, S, Pietrini, A M, Ricci, S.: Euendolithic activity of the cyanobacterium Chroococcus
779 lithophilus Erc. In biodeterioration of the Pyramid of Caius Cestius, Rome, Italy.
780 International Biodeterioration & Biodegradation, 100: 7-16,
781 <https://doi.org/10.1016/j.ibiod.2015.01.019>, 2015

782 Gorbushina, A. Lyalikova, N. Vlasov, D.Y. Khizhnyak, T.: Microbial communities on the
783 monuments of Moscow and St. Petersburg: biodiversity and trophic relations. Microbiology,
784 71, 350-356, <https://doi.org/10.1023/A:1015823232025>, 2002

785 Guiamet, P., Crespo, M., Lavin, P., Ponce, B., Gaylarde, C., Saravia, S. G. D.: Biodeterioration of
786 funeral sculptures in La Recoleta Cemetery, Buenos Aires, Argentina: Pre- and post-
787 intervention studies. Colloids and Surfaces B: Biointerfaces, 101: 337-342,
788 <https://doi.org/10.1016/j.colsurfb.2012.06.025>, 2013.

789 Guillitte, O., Dreesen, R: Laboratory chamber studies and petrographical analysis as bioreceptivity

790 assessment tools of building materials, *Science of The Total Environment*, Volume 167,
791 Issues 1–3, 365-374, [https://doi.org/10.1016/0048-9697\(95\)04596-S](https://doi.org/10.1016/0048-9697(95)04596-S), 1995

792 He, H.: Study on the Weathering of Marble Jinshi Steles in Beijing Confucius Temple. *Capital*
793 *Museum Forum*, (35): 226-231, 2021.

794 Hu, H., Wei, Y. (Editors).: *Systematics, Classification, and Ecology of Freshwater Algae in China*.
795 Beijing: Science Press. 23-203, 2006.

796 Isola, D., Zucconi, L., Onofri, S., Caneva, G., Selbmann, L.: Extremotolerant rock inhabiting black
797 fungi from Italian monumental sites. *Fungal Diversity* 76, 75–96.
798 <https://doi.org/10.1007/s13225-015-0342-9>, 2016

799 Jung, P., Baumann, K., Emrich, D., Springer, A., Felde, V. J. M. N. L., Dultz, S., Baum, C., Frank,
800 M., Büdel, B., Leinweber, P.: Lichens Bite the Dust – A Bioweathering Scenario in the
801 Atacama Desert. *iScience*, 23, 101647. <https://doi.org/10.1016/j.isci.2020.101647>, 2020

802 Komarek, J., Anagnostidis, K.: *Cyanoprokaryota* 1. Teil: Chroococcales. Vol. 19(1), In: Ettl H.,
803 Gaertner G, Heynig, H. and Mollenhauer, D. (eds.), *Suesswasserflora von Mitteleuropa*, Gustav
804 Fischer, Jena-Stuttgart-Luebeck:Ulm. 1-548. <https://doi.org/10.2216/i0031-8884-38-6-544.1>,
805 1998.

806 Komarek, J., Anagnostidis, K.: *Cyanoprokaryota* 2. Teil: Oscillariales. Vol. 19(2), In: Büdel B.,
807 Gärtnert G, Krienitz, L. and Schagerl, M. (eds.), *Suesswasserflora von Mitteleuropa*. Heidelberg,
808 Germany: Springer Spektrum. 1-759, 2005.

809 Komarek, J., Büdel, B., Gärtnert, G. *Süßwasserflora von Mitteleuropa*, Bd. 19/3: *Cyanoprokaryota*:
810 3. Teil / 3rd part: Heterocytous Genera. Springer Spektrum, 2013

811 Korkanç, M, Savran, A.: Impact of the surface roughness of stones used in historical buildings on
812 biodeterioration. *Construction and Building Materials*, 80: 279-294,
813 <https://doi.org/10.1016/j.conbuildmat.2015.01.073>, 2015

814 Lefler, F.W., Berthold, D.E., Laughinghouse, H. D.: *Cyanoseq*: A database of cyanobacterial 16S
815 rRNA gene sequences with curated taxonomy. *J. Phycol.*, 59: 470-480,
816 <https://doi.org/10.1111/jpy.13335>, 2023.

817 Leo, F., D., Antonelli, F., Pietrini, A., M., Ricci, S., Urzì, C.: Study of the euendolithic activity of
818 black meristematic fungi isolated from a marble statue in the Quirinale Palace's Gardens in
819 Rome, Italy. *Facies*, 65,18, <https://doi.org/10.1007/s10347-019-0564-5>, 2019

820 Li, J.: Research on mechanical properties evaluation and deterioration mechanism of heritage rock
821 in different environment. Master's Thesis. Beijing: Beijing University of Civil Engineering
822 and Architecture. 1-72. <https://link.cnki.net/doi/10.26943/d.cnki.gbjzc.2023.000478>, 2023.

823 Liu, J.: Experimental study of thermal effects on Physical-mechanical properties of Beijing
824 dolomitic marble. Master's Thesis. Beijing: China University of Geosciences (Beijing). 1-78.
825 <https://link.cnki.net/doi/10.27493/d.cnki.gzdzy.2020.001911>, 2020.

826 Lombardozzi, V., Castrignanò, T., Antonio, M. D., Municchia, A C, Caneva, G.: An interactive
827 database for an ecological analysis of stone biopitting. International Biodeterioration &
828 Biodegradation, 73: 8-15, <https://doi.org/10.1016/j.ibiod.2012.04.016>, 2012

829 Lü, J., Wei, J.: Contribution of Dashiwo Marble in Fangshan, Beijing to the Foundation of the
830 Forbidden City and Stone Sutras of Yunju Temple. Fossil, (03): 68-73, 2020.

831 Macedo, M F , Miller, A Z, Dionísio, A, Saiz-Jimenez, C: Biodiversity of cyanobacteria and green
832 algae on monuments in the Mediterranean Basin: An overview. Microbiology, 155(Pt 11): 3476-
833 3490. <https://doi.org/10.1099/mic.0.032508-0>, 2009

834 Marvasi, M., Cavalieri, D., Mastromei, G., Casaccia, A., Perito, B.: Omics technologies for an in-
835 depth investigation of biodeterioration of cultural heritage. Int. Biodeterior. Biodegrad., 144,
836 <https://doi.org/104736>, 10.1016/j.ibiod.2019.104736, 2019

837 Marvasi, M., Donnarumma, F., Frandi, A., Mastromei, G., Sterflinger, K., Tiano, P., Perito, B.: Black
838 microcolonial fungi as deteriogens of two famous marble statues in Florence, Italy,
839 International Biodeterioration & Biodegradation, Volume 68, 36-44,
840 <https://doi.org/10.1016/j.ibiod.2011.10.011>, 2012

841 Mascalchi, M., Osticioli, I., Cuzman, O. A., Mugnaini, S., Giamello, M., Siano, S.: Laser removal
842 of biofilm from Carrara marble using 532 nm: The first validation study, Measurement, V.
843 130, 255-263, <https://doi.org/10.1016/j.measurement.2018.08.012>, 2018

844 Miller, A., Dionísio, A., Macedo, M. F.: Primary bioreceptivity: A comparative study of different
845 Portuguese lithotypes. International Biodeterioration & Biodegradation, 57(2): 136-142.
846 <https://doi.org/10.1016/j.ibiod.2006.01.003>, 2006.

847 Miller, A.Z. Sanmartín, P., Pereira-Pardo, L., Dionísio, A., Saiz-Jimenez, C., Macedo, M.F., Prieto,
848 B.: Bioreceptivity of building stones: A review, Science of The Total Environment, Volume
849 426, 1-12, <https://doi.org/10.1016/j.scitotenv.2012.03.026>, 2012

850 Monte, M Del, Sabbioni, C.: Chemical and bioweathering of an historical building: Reggio Emilia
851 Cathedral. *Science of The Total Environment*, 50: 165-182, [https://doi.org/10.1016/0048-9697\(86\)90358-X](https://doi.org/10.1016/0048-9697(86)90358-X), 1986

852

853 Moropoulou, A, Bisbikou, K, Torfs, K, Van Grieken, R, Zezza, F, Macri, F.: Origin and growth of
854 weathering crusts on ancient marbles in industrial atmosphere. *Atmospheric Environment*,
855 32(6): 967-982, [https://doi.org/10.1016/S1352-2310\(97\)00129-5](https://doi.org/10.1016/S1352-2310(97)00129-5), 1998

856 Pinna, D, Galeotti, M, Perito, B, Daly, G, Salvadori, B.: In situ long-term monitoring of
857 recolonization by fungi and lichens after innovative and traditional conservative treatments
858 of archaeological stones in Fiesole (Italy), *International Biodeterioration & Biodegradation*,
859 Volume 132, 49-58, <https://doi.org/10.1016/j.ibiod.2018.05.003>, 2018

860 Pinna, D.: *Coping with Biological Growth on Stone Heritage Objects: Methods, Products,
861 Applications, and Perspectives* (1st ed.). Apple Academic Press.
862 <https://doi.org/10.1201/9781315365510>, 2017

863 Praderio, G., Schiraldi, A., Sorlini, C., Stassi, A., Zanardini, E.: Microbiological and calorimetric
864 investigations on degraded marbles from the Cà d'Oro facade (Venice). *Thermochimica Acta*,
865 227: 205-213. [https://doi.org/10.1016/0040-6031\(93\)80263-A](https://doi.org/10.1016/0040-6031(93)80263-A), 1993.

866 Qu, S.: The research on the weathering mechanism and weathering degree evaluation system of
867 marble relics in Beijing. Master's Thesis. Beijing: Beijing University of Chemical Technology.
868 1-140, 2018.

869 Santo, A., P., Agostini, B., Cuzman, O., A., Michelozzi, M., Salvatici, T., Perito, B.: Essential oils
870 to contrast biodeterioration of the external marble of Florence Cathedral, *Science of The Total
871 Environment*, V. 877, <https://doi.org/10.1016/j.scitotenv.2023.162913>, 2023,

872 Scheerer, S., Ortega-Morales, O., & Gaylarde, C.: Microbial deterioration of stone monuments—an
873 updated overview. *Advances in Applied Microbiology*, 66, 97–139,
874 [https://doi.org/10.1016/S0065-2164\(08\)00805-8](https://doi.org/10.1016/S0065-2164(08)00805-8), 2009

875 Tian, Y., Zhang, J., Song, L., Bao, H.: A study on aerial algae communities on the surface of
876 carbonate rock of the Yunnan stone forest. *Carsologica Sinica*, (03): 39-47, 2003.

877 Tian, Y., Zhang, J., Song, L., Bao, H.: A Study on Aerial Cyanophyta (Cyanobacteria) on the Surface
878 of Carbonate Rock in Yunnan Stone Forest, Yunnan Province, China. *Acta Ecologica Sinica*,
879 (11): 1793-1802+2020-2022, 2002.

880 Tian, Y., Zhang, J., Song, L., Bao, H.: The role of aerial algae in the formation of the landscape of
881 the Yunnan Stone Forest, Yunnan Province, China. *Science in China, Series D: Earth Sciences*,
882 47(9): 846-864., 2004.

883 Timoncini, A., Costantini, F., Bernardi, E., Martini, C., Mugnai, F., Mancuso, F. P., Sassoni, E.,
884 Ospitali, F., & Chiavari, C.: Insight on bacteria communities in outdoor bronze and marble
885 artefacts in a changing environment. *Science of the Total Environment*, 850,
886 <https://doi.org/10.1016/j.scitotenv.2022.157804>, 2022

887 Trovão, J., Portugal, A.: The impact of stone position and location on the microbiome of a marble
888 statue. *The Microbe*, 2, 100040. <https://doi.org/10.1016/j.microb.2024.100040>, 2024

889 Venturi, S., Tassi, F., Cabassi, J. , Gioli,B. , Baronti, S., Vaselli, O., Caponi,C. , Vagnoli,C.
890 Picchi, G., Zaldei, A., Magi, F., Miglietta, F. , Capecchiacci, F. : Seasonal and diurnal
891 variations of greenhouse gases in Florence (Italy): Inferring sources and sinks from carbon
892 isotopic ratios, *Science of The Total Environment*, Volume 698,
893 <https://doi.org/10.1016/j.scitotenv.2019.134245>, 2020.

894 Wang, F, Fu, Y, Li, D, Huang, Y, Wei, S.: Study on the mechanism of the black crust formation on
895 the ancient marble sculptures and the effect of pollution in Beijing area. *Heliyon*, 8(9):
896 e10442, 2022

897 Wang, S.: The characteristic analysis of surface deterioration and mechanism study on West Yellow
898 Temple Stone heritage. Master's Thesis. Beijing: China University of Geosciences (Beijing). 1-
899 57, 2010.

900 Warscheid, T., Braams, J.: Biodeterioration of stone: a review. *International Biodeterioration &*
901 *Biodegradation*, 46(4): 343-368, [https://doi.org/10.1016/S0964-8305\(00\)00109-8](https://doi.org/10.1016/S0964-8305(00)00109-8), 2000

902 Wu, M., Liu, J.: Fangshan Dashiwo and Stone Quarrying for Ming Dynasty Palaces and Tombs in
903 Beijing - Also on Stone Usage in Beijing's Imperial Construction Through Dynasties.
904 *Proceedings of the Palace Museum* (First Volume). 253-262, 1996.

905 Wu, Y., Zhang, B., Zhang, J., Zhai, K., Luo, L.: Weathering Characteristics of White Marble Relics
906 Around the Hall of Supreme Harmony (Taihe Dian) in the Forbidden City. *KSCE Journal of*
907 *Civil Engineering*, 27(2): 794-804, <https://link.cnki.net/doi/10.1007/s12205-022-1108-z>
908 2023.

909 Yang, X.: Study on Weathering mechanism of Beijing Marble. Master's Thesis. Beijing: China

910 University of Geosciences (Beijing): 1-92, 2016.

911 Ye, J., Zhang, Z.: Correlation Study of Physical and Mechanical Parameters of Beijing Marble.

912 Journal of Engineering Geology, 27 (3): 532-538.

913 <https://link.cnki.net/doi/10.13544/j.cnki.jeg.2018-102>, 2019.

914 Zhang, G.: Research on the weathering mechanism and Protection technology of spalling disease of

915 Marble relics in Beijing. Master's Thesis. Beijing: Beijing University of Chemical Technology.

916 1-77. <https://link.cnki.net/doi/10.26939/d.cnki.gbhgu.2022.000801>, 2022.

917 Zhang, T., Li, D., Zhang, Z.: Damage categories and deterioration mechanism of stone cultural relics

918 of white marble in Beijing. Geotechnical Investigation & Surveying, 44 (11): 7-13, 2016.

919 Zhang, Z., Yang, X., Ye, F., et al.: Microscopic characteristics of petrography and discussion on

920 weathering mechanism of Fangshan marble in Beijing. Journal of Engineering Geology, 23

921 (02): 279-286. <https://link.cnki.net/doi/10.13544/j.cnki.jeg.2015.02.013>, 2015.

922 Zheng, L., Li, K., Wang, J., Li, L., Wang, Y., Wang, M.: Investigations on the surface deterioration

923 process and mechanisms of white marble. Construction and Building Materials, 472: 140844,

924 <https://link.cnki.net/doi/10.1016/j.conbuildmat.2025.140844>, 2025

925 Zhu, H.: Freshwater Algae in China (Volume 2, Orders Chroococcales). Beijing: Science Press. 1-

926 105, 1991.

927

928

929

930